Journal of Energy

ISSN 1849–0751 (On–line)
ISSN 0013–7448 (Print)
UDK 621.31

https://doi.org/10.37798/EN2023722

VOLUME 72 Number 2 | 2023

ENERGIJA 72

Journal of Energy

Scientific Professional Journal Of Energy, Electricity, Power Systems
Online ISSN 1849–0751, Print ISSN 0013–7448, VOL 72
https://doi.org/10.37798/EN2023722

Published by
HEP d.d., Ulica grada Vukovara 37, HR–10000 Zagreb
HRO CIGRÉ, Berislavićeva 6, HR–10000 Zagreb

EDITORIAL

The first paper is “Monitoring Transformer Condition with MLP Machine Learning Model”. This paper presents the development and potential application of a transformer winding temperature model using artificial neural networks. The model, implemented in Python, utilizes data collected over one year for a single transformer. Three input features are used to predict the winding temperature: oil temperature, winding current, and outside temperature. The model demonstrates good accuracy, except for extreme outliers and sudden changes in winding current which can cause larger errors. However, these errors are not significant and do not affect the overall performance of the model. Further improvements can be made by reducing absolute error, testing more sensitive indicators, exploring different activation conditions, and using moving window statistical measures. Real-time testing and exploring alternative machine learning approaches could enhance the model’s accuracy and applicability. Factors such as active cooling, power flow direction, and power ratios could also be considered to improve the model.

The second paper is “Characterization of Fast Neutron Transmission Through an Iron Shield”. This paper focuses on the analysis of neutron transmission through an iron sphere using Monte Carlo and transport theory methods based on the ENDF/B-VII.1 general purpose library. The investigation aims to address deficiencies in the iron inelastic data from the older library evaluation (ENDF/B-V) and its impact on neutron flux underestimation in reactor pressure vessels. Experimental data from neutron leakage spectra experiments conducted in the 1990s are used to benchmark the next-generation ENDF/B-VI iron data. The study utilizes a hybrid shielding methodology and compares dosimeter activation rates calculated with the MCNP6.1.1b code using different nuclear data libraries. The results indicate increased neutron transmission in iron at energies above 1 MeV with the updated ENDF/B-VII.1 evaluation. Detector reaction rates show good agreement, with higher rates observed for high-energy threshold reactions. The findings demonstrate the performance of the recommended dosimetry library (IRDFF-II) compared to previous versions (IRDFF-1.05). The paper extends the previous work and provides insights into neutron transmission in iron and its impact on reaction rates.

The third paper is “A Comparative Analysis of Electric Mobility Operations in the Island States: A Case Study of Malta and Cyprus”. The Malta and Cyprus partnership has been strengthened through the H2020 NEEMO TWINNING project, promoting collaboration and sustainable transportation in the electric mobility sector. Capacity-building activities, including workshops, seminars, and exchange visits, have helped characterize the state of the electric transportation industries in both island nations. The research emphasizes the importance of sustainable energy sources and infrastructure development for a smooth transition to electric mobility. Various aspects such as energy systems, land transportation, and optimizing the entire energy system are discussed, compared, and analyzed. The study explores legal frameworks, the EIRIE platform, differences between Malta and Cyprus in the e-mobility sector, and the integration of renewable energy and charging infrastructure. The findings underscore the need for accelerating the transition to electric vehicles in line with EU regulations. The study provides valuable insights into the electric mobility market in Malta and Cyprus, aiming to foster environmentally friendly and sustainable transportation while supporting the EU’s goals.

The fourth paper is “Seismic standards qualification of instrument transformers by shake table test and linear FEM analysis”. This paper focuses on seismic qualifications and the preparation, implementation, and supervision of seismic tests conducted on instrument transformers. The study follows the standards set by IEEE 693, a demanding seismic standard for substation equipment, and compares it to other relevant standards for a comprehensive perspective. Finite element method (FEM) analysis is utilized as a tool for design preparation, pre-test analysis, and seismic qualification. The paper draws on findings from seismic tests conducted on different transformers in various test laboratories, forming the basis for detailed analysis and insights aligned with IEEE 693. The article aims to provide a comprehensive understanding of the seismic qualification process, offering valuable insights for substation designers, seismic specialists, and end users. It also establishes a foundation for further research in the seismic performance of instrument transformers.

Igor Kuzle
Editor–in–Chief

Journal of Energy
VOLUME 72 Number 2 | 2023
journal homepage: http://journalofenergy.com/

Monitoring Transformer Condition with MLP Machine Learning Model

Dino Žanić, Alan Župan

***Summary* — Failures of large power transformers in transmission system are always followed by significant costs, which is especially problematic given that they present an unplanned expenditure. In addition from disrupting financial plans, these events can lead to lower system reliability. This paper describes the development and potential application of transformer winding temperature model based on multilayer perceptron class of artificial neural networks. Model is built in Python programming language with data collected over the span of one year for a single transformer. Three input features (oil temperature, winding current and outside temperature) are used in the input layer, aiming to predict the winding temperature in the transformer. By comparing the predicted winding temperature with the actual measured winding temperature, insights into the transformers internal condition can be derived. To demonstrate the models proposed application, two types of transformer condition degradation are simulated and a set of certain indicators based on statistical measures are explored.**

***Keywords* — transformers, artificial neural networks, condition monitoring**

I. Introduction

TRANSFORMERS are exceptionally crucial components of the transmission network. Their uninterrupted operation (aside from planned maintenance) is vital for stability and reliability of electric power system (EPS). Failures not only have the potential to interrupt the customer supply and damage to other assets, but under certain circumstances can lead to ripple effect that impacts EPS across various countries or regions. Repercussions of these events, when quantified, are always associated with high material costs. However, they can also result in indirect loss of life and reputational damage which can't be easily quantified, but nonetheless carry immense significance [1-4]. Given the risks, transmission operators have the responsibility of ensuring the continuous operation of transformers. Therefore, any novel and promising approaches like vibro-acoustic diagnostics [5] and machine learning applications [6] that could further this goal warrant a thorough examination.

The model is based on multilayer perceptron (MLP), a fundamental class of artificial neural networks (ANN). MLPs are widely used due to their flexibility and large number of evolutions that have evolved from them [7-9].

(Corresponding author: Dino Žanić)
Dino Žanić and Alan Župan are with Croatian Transmission System Operator d.d. (HOPS), Kupska 4, 10000 Zagreb, Croatia
(e-mails: dino.zanic@hops.hr, alan.zupan@hops.hr).

In this case, the MLP is characterized by three features in the input layer and a single label as the output layer. The model is used to predict the winding temperature based on winding current, oil temperature and outside temperature.

Oil temperature is used as an input given that the transformer oil acts as a heatsink with inherent inertia. This affects the dynamics between changes in winding current and winding temperature, primarily because the efficiency of heat transfer between the transformer windings and the oil is directly proportional to their temperature difference. The same principle applies to the air temperature outside the transformer and transformer oil. The intent is that these temperature ratios, which capture the systems cooling efficacy, are encapsulated within the architecture of the neural network.

Predicted temperature is further compared with the measured temperature to ascertain the difference between them. Change in their discrepancy over time can serve as an indicator or set of indicators for the transformers internal condition. This can be used to: identify an ongoing negative process inside the transformer which enables timely action to prevent a future failure, serve as a long-term condition monitoring indicator for age and degradation based replacement planning or track and analyze the severity and consequences of adverse effects resulting from various damaging events.

The input features used in the model are typical and often widely available in transmission operators. Data for this model was acquired from Croatian transmission system operators SCADA system and a meteorological station located in the same transformer station. Basic data pertaining to the transformer under study is presented in Table I, while the corresponding image is provided in Fig. 1.

Table I

Basic Transformer Data

Rated Power	300 000/300 000/(100 000) kVA
Rated Voltage	400 000/115 000/(10 470) V
Rated Current	433.0/1 506.1/(5 514.3) A
Frequency	50 Hz
Connection Group	YNaO(d5)
Cooling Type	OFAF

The data required extensive processing and preparation before the model could be developed. This was done using Python programming language with the help of scikit-learn [10-11] framework and various other libraries. Finally, various hyperparameters of

Dino Žanić, Alan Župan, Monitoring Transformer Condition with MLP Machine Learning Model, Journal of Energy, vol. 72 Number 2 (2023), 3–7
https://doi.org/10.37798/2023722417

the model were optimized over multiple iterations to achieve the best possible results. As actual faults are infrequent and only newer transformers have available internal temperature data, examples where all input data is available during faults is scarce. For that reason, two types of faults are simulated to demonstrate models suggested application.

Fig. 1. Image of the transformer from which the data was collected

II. Data Preparation

A. Data preprocessing

As winding temperature is a continuous variable, the problem of modelling falls under the category of regression problems. The data set has to be prepared in such a way where incomplete entries are removed. To achieve this, it is first necessary to synchronize all data points and prune the data set. Any missing timestamps must first be found and filled in for every input feature, which is then followed by trimming of certain features to a common sampling frequency. Finally, the features are time synchronized after which it is possible to remove entries with partially available data.

Justification for removal of entries where data is not available for each feature lies in the fact that the ANN lacks a memory module. Every training pass of the ANN updates its weights, which means that all previous states are embedded in the numerical value of the updated weights. For that reason, there is no value in feeding fabricated data to the ANN as it only degrades the ANN performance with regards to real data. In fact, it can be argued that classical interpolation of the missing data falsely inflates the precision of the ANN if the interpolation is used on both training and testing sets, as it introduces bias.

Winding current, oil temperature and winding temperature were all available in 15-minute sampling frequency at best, while the outside temperature data was available every 1-minute. For this paper, one year of data for a single transformer was taken which after preprocessing resulted in 512,683 individual data points for outside temperature and 35,041 data points for each feature and target label. Because this amount of data would be very hard to process conventionally, custom algorithms were applied to the data set in order to expedite this stage of data preparation.

There are two instances in the data set where the winding temperature sensor measures 0°C, coinciding with current values of 0 A. However, there are other instances in the dataset where current through the windings also reads 0 A, but the winding temperature remains unaffected. This suggests that the two data points in question are a result of a possibly systematic failure in the data collection, that simultaneously impacted both sensors.

These data points were not excluded from the data set, as it can be valuable to study the behavior of the model during short-term sensor failure. The reduction in the error from the first iteration, even when the data from two sensors was faulty indicates that the model has enhanced robustness to outliers and is not overfitting. This is especially important as it indicates that the short-term sensor failures or data collection issues will not adversely affect the indicators, which are discussed further in the paper.

B. Data processing

This phase of data preparation refers to processing of the data for the ANN. It is conducted in the same Python script where the very MLP model is built, as the processing time is negligible in comparison to the training time of the model. The optimal range of input data for the ANN is between 0 and 1, which means that the data has to be normalized. The min-max scaling algorithm is applied on the data set to preserve the original relative distances between the data points, and sets the data in the preferred range for the ANN. Min-max scaling normalization is described by:

$$X' = \frac{X - X_{\min}}{X_{\max} - X_{\min}} \tag{1}$$

where X' is the scaled value, X is the value to be scaled, X_{min} is the minimum value of the corresponding feature data set and X_{max} is the maximum value of the corresponding feature data set. Finally, the script splits the data set into data for training, testing and validation.

III. Model Training and Optimization

MLP models are characterized by many hyperparameters (HPs) which can roughly be divided between: model HPs, optimization algorithm HPs and backpropagation algorithm HPs. In order to validate the model accuracy, two common statistical measures were employed, mean squared error (MSE) value of which should be minimized and determination coefficient (R2), which should be maximized.

A. First iteration

The initial iteration of the model with mostly default settings already gives promising results with MSE of 0.79 and R2 of 0.978. However, it doesn't converge over 200 iterations and exhibits a peak error exceeding 50°C in a specific case where the temperature and current measurement sensors experience a malfunction. This suggests that the model is overfitting and robustness is low, as anomalous data causes significant errors.

The default topological construction of this model consists only of input and output layer with 100 neurons in a single hidden layer.

Example shown in Fig. 2 illustrates modelled winding temperature represented by the red curve, and measured winding temperature represented by the blue curve. As well as differential error between the modelled and measured values which is represented by the green curve.

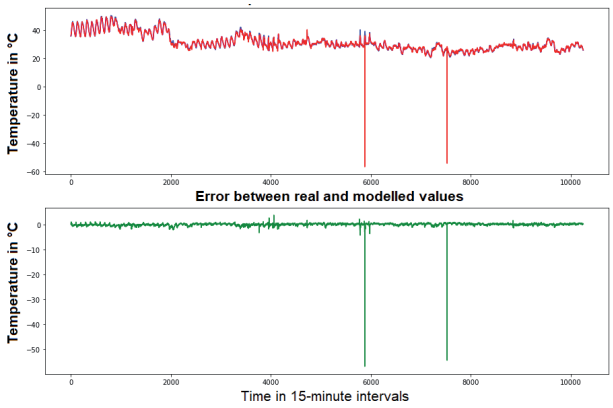

Fig. 2. Comparison of real and modelled winding temperature for default model

B. Optimization process

As mentioned earlier, many different HPs are being fine-tuned during the optimization process. Given that the sample space for each HP is virtually infinite, it's necessary to establish limitations for both the sample space and the sample step for each HP. Certain HPs which belong to the same group are interdependent, which implies that groups of interdependent HPs should be optimized at the same time. Yet, even if we limit their sample space and sample step, there can still be millions of different HP combinations.

To manage this, HPs are initially sampled using a fairly large step. Once the best combination is found, sample space around the best HP values is resampled, effectively increasing the resolution. In this way, after several cycles of HP fine-tuning, the local optimum is reached where further sampling doesn't yield significant improvements to the model performance.

Due to the large sample step initially employed in the optimization process, there is a risk that the resulting optimum is local rather than local, which can be addressed in many ways, but only with an increase in optimization time.

Model optimization doesn't only increase the model accuracy, but it is usually followed by faster training convergence. A characteristic which can be optimized for if it is necessary for the application.

C. Final model

The results of the final model are shown in Fig. 3, where modelled and measured values of winding temperature are again represented by red and blue curves, respectively.

Fig. 3. Comparison of real and modelled winding temperature for optimized model

Having reached full parametrization, the model no longer benefits from further fine-tuning in terms of relevant increase to the precision or convergence speed. The final model adopts the following topology: 3 neurons in the input layer, 38 neurons in the first hidden layer, 7 neurons in the second hidden layer and 1 neuron in the output layer. Full convergence is reached after 153 iterations achieving a MSE of 0.189 and R2 coefficient of 0.995. Notably, when compared with the first iteration, the errors represented by the green curve in Fig. 3, are significantly smaller in cases where current values undergo sudden changes, or even when the model encounters anomalous data.

During training, the majority of the improvement in minimization of the loss function occurs in the first 10 iterations, ensuring high accuracy. While the remaining training iterations are dedicated to achieving high precision of the model.

IV. Demonstration

A. Simulated condition deterioration

In order to demonstrate the main use case of the model, two distinct deteriorating conditions were simulated. For the simulations, an exponential variable was added to the measured winding temperature, which preserves the pattern of the series but exacerbates the overall shape to simulate a positive feedback loop of gradual worsening of the condition.

Fig. 4 and Fig 5. demonstrate comparisons between the modelled and simulated deteriorating winding temperatures represented again by red and blue curves, respectively. While the differential error between these curves is depicted by the green curve.

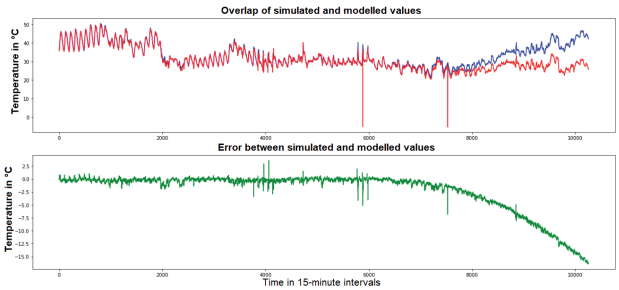

Fig. 4. Comparison of simulated gradually deteriorating and modelled winding temperature

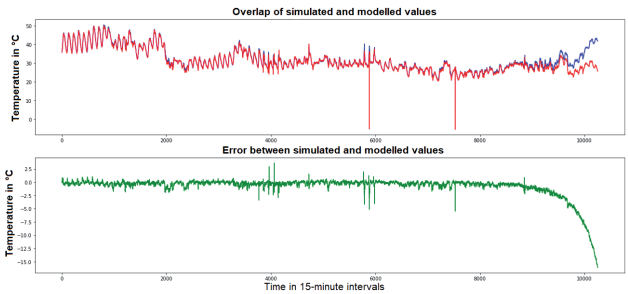

Fig. 5. Comparison of simulated suddenly deteriorating and modelled winding temperature

Both simulations commence exactly 42 days before the end of the data set as indicated by red vertical line in Fig. 6 and Fig. 7. The first example simulates a gradual deterioration of the condition, while the second example simulates at first a very minor imper-

Dino Žanić, Alan Župan, Monitoring Transformer Condition with MLP Machine Learning Model, Journal of Energy, vol. 72 Number 2 (2023), 3–7
https://doi.org/10.37798/2023722417

ceptible deterioration of the condition which at one point causes a runaway effect. These simulations are further used to demonstrate and explore the systems capability to detect discrepancies between the modelled and measured values, as well as its sensitivity.

B. Discrepancy detection and indicators

While a human observer could detect divergence between modelled and measured winding temperatures, triggering further investigation into the condition of the transformer, that approach rests on inherent unreliability of human perception, judgement and diligence in monitoring. Thus, an alternative approach using statistical indicators is proposed. This approach, based on common statistical principles, generates limits automatically from past values to detect changes in trend.

The first part of the process in creating the indicators involves using a moving window with three different widths: one day, one week and one month. With each new measurement, these windows shift forward, adding average, standard deviation, and median values to their respective lists.

The second part of the indicator is its activation function, which tracks the average, maximum, minimum and median values of each list. After a new measurement is taken (in this case every 15 minutes) and lists are updated, the activation function compares the new value being added to the list against the average, maximum, minimum and median values of the whole list. If, for example, the new value is a new maximum median in the daily medians list, the corresponding indicator would be triggered. For this purpose, a total of 36 indicators were created. However, due to practical considerations, only a select number of these indicators are presented in this paper.

These indicators were not envisioned to function individually, but rather in tandem, as different indicators track changes in different timeframes, and different activation functions have different sensitivities. In practice, it would also be advisable to confirm that these activations were not a anomalies by observing successive indicator activations for a desired timeframe. These statistical measures and their respective activation functions can detect a deterioration in the condition far sooner and with firmer evidence than a human observer relying solely on visual comparison of the modelled and real winding temperature.

1) Simulation of gradual condition deterioration

Fig. 6 presents four separate graphs each representing a specific statistical measure. Each graph contains three curves each depicting a specific time interval in which corresponding statistical measures are taken: daily interval in purple, weekly interval in orange and monthly interval in cyan. These curves subsequently serve as lists of values upon which activation conditions of individual indicators are applied.

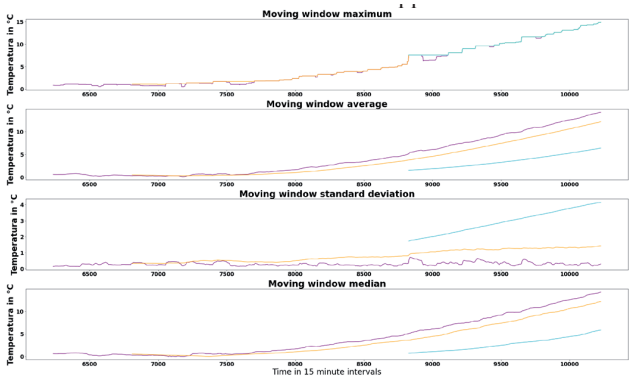

Fig. 6. Moving window curves of maximum, average, standard deviation, and median differential error in winding temperature over daily, weekly, and monthly intervals

Table II of indicator performance highlights the earliest activation times for indicators from the gradual condition simulation group.

Table II

Indicator Performance for Simulated Gradual Condition Deterioration

List	Activation	Time
AVG(d)	max	16d 10h
AVG(w)	max	17d 7h
STD(d)	avg	9d 17h
STD(w)	avg	11d 14h
STD(m)	max	12d 15h
MED(d)	max(min)	11d 23h
MED(d)	med	3d 17h
MED(w)	max(min)	14d 7h
MED(w)	med	8d 21h
MED(m)	max(min)	21d 22h

In case of gradual condition deterioration, the average activation time for the better performing indicators is about 11 days, or as shown in Fig. 7 by the light green curve, at 4.29% deviation between the model and simulation. After 12 days and 15 hours, six indicators would be activated which would strongly indicate the existence of a progressive negative process in the transformer which is indicated by the brown vertical line.

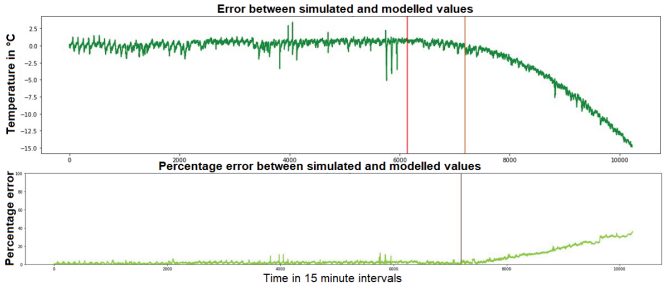

Fig. 7. Average activation time of indicators for simulated gradual condition deterioration visualized on absolute and percentage errors

2) Simulation of sudden condition deterioration

Fig. 8 again presents four separate graphs each representing a specific statistical measure, where each graph contains three curves depicting daily, weekly and monthly time intervals for corresponding statistical measures in purple, orange and cyan, respectively. As in the case of previous simulation, these curves subsequently serve as lists of values upon which activation conditions of individual indicators are applied.

Earliest activation times of indicators belonging to the simulation of sudden condition deterioration group are shown in Table II.

The average activation time of indicators for the simulated case of sudden condition deterioration is 32 days, or as shown in the Fig. 9 by the light green curve, at 2.08% of deviation between model and simulation values. However, when values around the moment of activation are observed, the deviation is similar to the value in the case of gradual condition deterioration. After 33 days and 21 hours from the start of the simulated deterioration, nine indicators would be activated which would present a very strong indication of the existence of a progressive negative process in the transformer.

Dino Žanić, Alan Župan, Monitoring Transformer Condition with MLP Machine Learning Model, Journal of Energy, vol. 72 Number 2 (2023), 3–7
https://doi.org/10.37798/2023722417

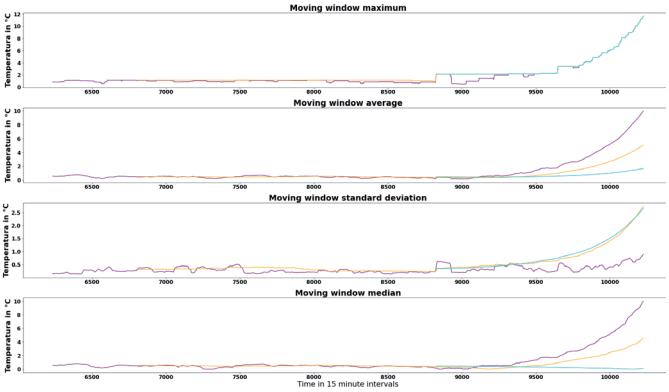

Fig. 8. Moving window curves of maximum, average, standard deviation, and median differential error in winding temperature over daily, weekly, and monthly intervals

TABLE III

INDICATOR PERFORMANCE FOR SIMULATED SUDDEN CONDITION DETERIORATION

It is notable that two indicators perform significantly better

List	Activation	Time
AVG(d)	max	33d 21h
AVG(w)	max	35d 7h
STD(d)	avg	9d 18h
STD(w)	avg	31d 13h
STD(m)	max	33d 13h
MED(d)	max(min)	33d 11h
MED(d)	med	3d 18h
MED(w)	max(min)	33d 8h
MED(w)	med	27d 8h
MED(m)	med	32d 23h

than the rest, which deserves further investigation into their applicability and consideration if they are prone to false-positive activation. Delayed times of activation are expected as the negative process in the second simulation starts off much slower, but ramps up in intensity significantly at a certain point in time.

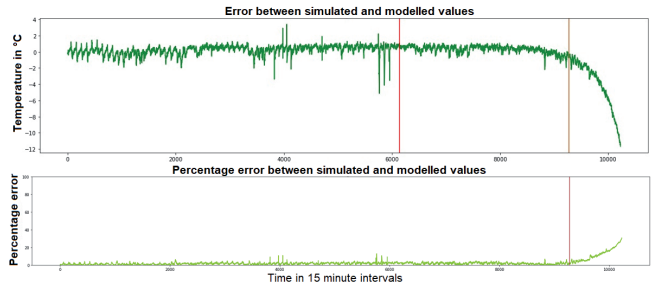

Fig. 9. Average activation time of indicators for simulated sudden condition deterioration visualized on absolute and percentage errors

V. CONCLUSION

This approach to modelling of transformer winding temperature proves to be fairly accurate, with only extreme outliers and sudden changes in the winding current causing larger errors. These instances do not present a significant issue as the errors are neither large nor long-lasting. Additionally, the indicators are resistant to errors as they are based on statistical measures which smooth out any outliers given that they are infrequent enough to still be considered as outliers. Furthermore, the very purpose of indicators is to spot long-term changes in the trends within the transformer and not single outliers.

Despite the models effectiveness, there could be room for further improvement. Should the models accuracy be enhanced by reduction in absolute error, the indicators would be more sensitive to the deviations between the real and modelled winding temperature. More sensitive indicators should be tested for false positives, and exploration of different indicator activation conditions as well as moving window statistical measures could yield further benefits.

The approach merits real-time testing to validate its proposed applicability. Several steps could be taken to further enhance the model's accuracy. For instance, exploring certain other approaches to machine learning could yield a more accurate model. Variables such as state of active cooling, direction of power flow or ratios between real and reactive power could increase the accuracy of the model.

Looking ahead, the process of data gathering and processing can be algorithmically automated. This coupled with novel approaches to machine learning could open the the possibility to create general models for transformers belonging to the same line of products.

REFERENCES

[1] B. Filipovic-Grcic, B. Jurisic, S. Keitoue *et al.*, *„Analysis of Overvoltages on Power Transformer Recorded by Transient Overvoltage Monitoring System"*, 5th International Colloquium on Transformer Research and Asset Management, Lecture Notes in Electrical Engineering, vol 671, Springer, Singapore, pp. 85-102, July 2020

[2] A. EL-Bassiouny, M. EL-Shimy, R. Hammouda, *„Impact of Power Transformer Failures on Customer Interruptions Costs Using Customer Damage Functions"*, 19th International Middle East Power Systems Conference (MEPCON 2017), Cairo, Egypt, 19-21 December 2017

[3] S. T. Jan, R. Afzal, A. Z. Khan, *„Transformer Failures, Causes & Impact"*, International Conference on Data Mining, Civil and Mechanical Engineering, Bali, Indonesia, 1-2 February 2015

[4] J. Singh, S, Singh, *„Transformer Failure Analysis: Reasons and Methods"*, International Journal of Engineering Research & Technology, Advanced Computational Methods in Electrical Engineerring 2016, Vol. 4, No. 15, 2016

[5] A. Secic, M. Krpan, I. Kuzle, *„Vibro-Acoustic Methods in the Condition Assessment of Power Transformers: A Survey"*, IEEE Access, Vol. 7, pp. 83915-83931, 2019

[6] A. E. Nezhad, M. H. Samimi, *„A review of the applications of machine learning in the condition monitoring of transformers"*, Energy Systems, Springer, 2022

[7] T. Hastie, R. Tibshirani, J. Friedman, *„The Elements of Statistical Learning – Data Mining, Inference and Prediction"*, Second edition, Springer, Stanford, California, August, 2008

[8] C. M. Bishop, *„Pattern Recognition and Machine Learning"*, First edition, Springer, Cambridge, England, February, 2006

[9] M. Minsky, S. Papert, *„Perceptrons – An Introduction to Computational Geometry"*, First Edition, The MIT Press, Cambridge, Massachusetts, and London, England, 1969

[10] F. Pedregosa et al., 1309.0238, *„Scikit-learn: Machine Learning in Python"*, Journal of Machine Learning Research, Vol. 12, pp. 2825–2830, 2011

[11] L. Buitinck et al., *„API design for machine learning software: experiences from the scikit-learn project"*, European Conference on Machine Learning and Principles and Practices of Knowledge Discovery in Databases, Prague, Czech Republic, September 2013

Journal of Energy
VOLUME 72 Number 2 | 2023
journal homepage: http://journalofenergy.com/

Characterization of Fast Neutron Transmission Through an Iron Shield

Mario Matijević, Krešimir Trontl, Dubravko Pevec

Summary **— In this paper we give an analysis of the neutron transmission through an iron sphere using Monte Carlo and transport theory methods based on ENDF/B-VII.1 general purpose library. The motivation for this investigation comes from a well-known deficiency in the iron inelastic data from the older library evaluation (ENDF/B-V), giving a concern for a fast neutron flux underestimation within the reactor pressure vessels. In order to benchmark the next-generation ENDF/B-VI iron data, the U.S. Nuclear Regulatory Commission and the former Czechoslovakian National Research Institute have jointly preformed several experiments in 1990s, addressing neutron leakage spectra obtained for a ^{252}Cf fission source in a centre of an iron sphere. It was shown that the ENDF/B-VI iron cross section, containing several improvements over previous evaluations, will not entirely resolve the neutron spectrum discrepancies observed at high neutron energies. Since safety analyses of reactor pressure vessel embrittlement are often based on neutron transport calculations using specific multigroup cross section libraries, simulation of this benchmark was performed using a hybrid shielding methodology of ADVANTG3.0.3 and MCNP6.1.1b codes. Comparison of calculated and referenced dosimeter activation rates are presented for several »standard« nuclear reactions, often used in reactor pressure vessel dosimetry. For that purpose, the new IRDFF-II special library from the IAEA Nuclear Data Services was used as a reference source of dosimetry cross sections. The MCNP6.1.1b code was used for calculation of reaction rates, which were also compared with previous IRDFF-1.05 special library and general purpose ENDF/B-VII.1 library.**

Keywords **— dosimetry, shielding, Monte Carlo, MCNP, ADVANTG**

I. Introduction

Before releasing the ENDF/B-VI general purpose cross section library there has been a reasonable concern that deficiencies in the iron inelastic scattering data may cause an underestimation in the calculated fast neutron flux within the reactor pressure vessels (RPVs) of power reactors [1]. At that time most of the USA safety analyses of RPV embrittlement were based on transport calculations with multigroup energy structure for obtaining fast neutron fluence inside the vessel regions. Validation of such transport solutions with measured dosimeter activation rates in the ex-vessel cavity region often indicated underestimation of calculated fast flux by up to 30% [1], directly influencing expectation value for reactor operational lifetime. With the release of ENDF/B-VI library some 30 years ago, an improvement in iron evaluations for cross sections above 1 MeV came along with the following:

1. correlation between incident neutron energy and forward bias in the angular distribution for inelastic scattering;
2. a reduction in the magnitude of the inelastic cross section data in the fast neutron region.

Initial data testing of the ENDF/B-VI iron data was done by Williams et al [2], but resulting in large discrepancies of measured and calculated neutron leakage spectra above 1 MeV from an iron sphere containing deuterium-tritium (DT) source of neutrons with 14.1 MeV. Clear conclusions of that experiment were not reached, except that interaction of 14.1 MeV neutrons in iron were quite different compared to a moderated fission spectrum incident on RPV of commercial PWR plants. This difficulty was overcome in the next phase of benchmarking the ENDF/B-VI iron data described by Sajo et al [1] using a new experimental configurations. The U.S. NRC and the former Czechoslovakian National Research Institute (NRI) in Rež (Czech Republic) have jointly conducted calculation and measurement of neutron leakage spectra from a ^{252}Cf fission source located at the centre of an iron sphere. The spontaneous fission spectrum of ^{252}Cf is similar to a hardened ^{235}U fission spectrum but without the $1/E$ slowing-down component, important for low energy threshold dosimeters. The paper [1] gives detailed comparison of calculated and experimental results, with major finding that the ENDF/B-VI cross sections improve fast neutron transmission through iron, but at the same time will not entirely resolve the neutron spectrum underestimation compared to experimental data for neutron energies above 1 MeV.

This paper presents a revision of this research using modern computational tools of particle transport. The Monte Carlo (MC) simulation of fast neutron transmission through an iron sphere was performed for the dual purpose:

1. testing of iron transport cross section data contained in the general purpose ENDF/B-VII.1 cross section library [3] and direct comparison with older ENDF/B-VI evaluation;
2. testing special dosimetry libraries IRDFF-II [4] and IRDFF-1.05 [5] with several reactions covering thermal, epithermal and fast neutron region to be used as a response functions on point detector 1 m away from the centre of the iron sphere.

(Corresponding author: Mario Matijević)
Mario Matijević, Krešimir Trontl and Dubravko Pevec are with the University of Zagreb Faculty of Electrical Engineering and Computing (FER), Zagreb, Croatia (e-mails: mario.matijevic@fer.hr, kresimir.trontl@fer.hr, dubravko.pevec@fer.hr)

The rest of the paper is organized as follows. Section 2 gives the experimental description and original calculations. The computational tools ADVANTG and MCNP are given in Section 3, together with a simulation model description. Section 4 gives results and discussion, while Section 5 gives conclusions. The referenced literature is given at the end of the paper.

II. Original Experiment Description

The original set of experiments was performed using iron spheres of various sizes with a small neutron source of ^{252}Cf located at the geometrical centre. The reference paper [1] and this paper are analysing one specific case, which is an iron sphere with an outer radius of 25 cm. Two independent measurements (NRI and Skoda Company) of the fast neutrons leaking from the surface of the iron sphere were done using a proton-recoil detector and a stilbene crystal spectrometer located at 100 cm from the source location. No detailed information about the detector configuration was provided in paper [1], but schematic diagram of experimental setup and central section of the source were included and are depicted here in Figure 1 and Figure 2 for the purpose of completeness.

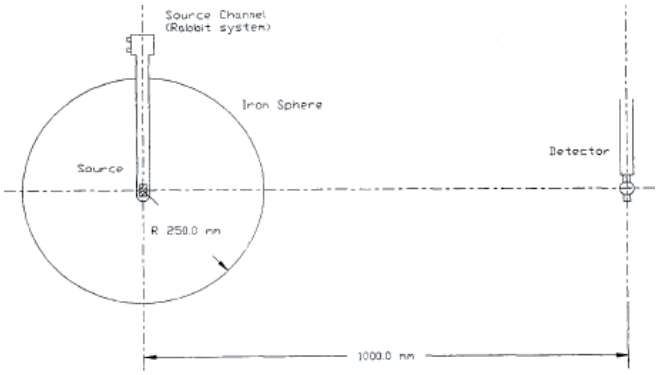

Fig. 1. Experimental setup for iron sphere and point detector [1]

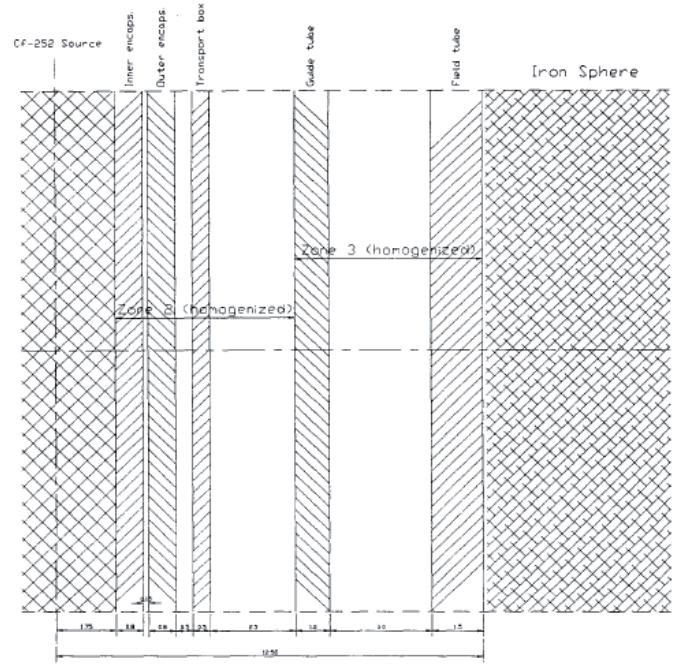

Fig. 2. Enlarged central section of the rabbit system housing the 252Cf source [1]

The safe handling of the neutron source was achieved by the so-called rabbit system, which consists of two concentric cylindrical tubes, movable guide tube inside a fixed field tube. The tubes and transport box enclosing the source are made from aluminium alloy. The ^{252}Cf source is in a form of a cylinder with 0.35 cm in diameter and 1.2 cm in height and has a double stainless-steel encapsulation. The dimensions of rabbit system tubes, transport box, steel encapsulation and cylindrical source can be found in [1] with material compositions of various elements, which were used as an input data for computational model preparation.

The reported neutron transport calculations were done using the one-dimensional discrete ordinates (SN) computer code XSDRNPM-S in a spherical geometry. For that purpose, the central cylindrical region of the experimental configuration was modelled as three separate homogenized spherical zones:

Zone 1: containing the source (void region);

Zone 2: containing source encapsulation and transport box;

Zone 3: capturing the rabbit system.

The spherical symmetry throughout the model geometry thus comprises of iron shield with the inner radius of 1.25 cm and with the outer radius of 25.0 cm. The SN mesh interval size was 0.16 cm with S16/P3 parameters taken for the quadrature set and the Legendre expansion of the scattering cross sections. The calculations were performed using 174 energy groups with the new ENDF/B-VI iron data, while keeping cross sections of other material unchanged, i.e. from previous evaluation. The resonance self shielding calculations based on Bondarenko method were performed with the computer program BONAMI-S. The fission spectrum of ^{252}Cf source was used from the National Institute of Standards and Technology (NIST), but additional details were not provided. The source strength was normalized to produce a neutron flux value of 1.0 n/cm^2/s at the location of point detector (r=100 cm) without the iron shield giving in turn source intensity of 125664 n/s. The computed neutron leakage spectrum at detector location enabled calculation of various reaction rates (i.e. integral responses) for different threshold detectors, while reactions of user interest presented in Table 1 are typical for RPV dosimetry. These reactions of interest were used as a neutron response functions in transport calculations of dosimeter reaction rates and were originally processed from the ENDF/B-V dosimetry file. The VITAMIN-E cross section library also contains these reactions and it was mentioned how the ^{63}Cu(n,α) cross section is known to be too large [1].

Table 1

Evaluated integral responses

Reaction of interest	Threshold energy (MeV)
^{63}Cu(n,α)	4.7
^{54}Fe(n,p)	2.3
^{58}Ni(n,p)	2.1
^{238}U(n,f)	1.5
^{237}Np(n,f)	1.2
^{59}Co(n,g)	thermal

III Computational Methods

The hybrid shielding approach combining deterministic-stochastic solution was used for this shielding problem. The discrete ordinates (SN) solution was obtained using the 3D deterministic transport solver Denovo [6] for adjoint, mesh-based variance reduction (VR) preparation. Using such VR parameters, the final, optimized and accelerated MC calculation can be performed. The Denovo SN solver is implementing Consistent Adjoint Driven Importance Sampling (CADIS) and Forward Weighted CADIS

Mario Matijević, Krešimir Trontl, Dubravko Pevec, Characterization of Fast Neutron Transmission Through an Iron Shield, Journal of Energy, vol. 72 Number 2 (2023), 8–14
https://doi.org/: 10.37798/2023722471

(FW-CADIS) methodologies [7], developed at Oak Ridge National Laboratory (ORNL). It is a very fast and robust SN solver, working with structured Cartesian grid implementing the Koch-Baker-Alcouffe (KBA) parallel transport sweep algorithm across structured meshes. The most important feature is multigroup flux positivity with positive scattering source and Step Characteristic (SC) spatial differencing option (default option), which is a basis for numerical stability of final MC simulation.

A. Hybrid shielding methodology

The ADVANTG3.0.3 [8] is an automated tool for generating VR parameters for a fixed-source continuous-energy Monte Carlo simulations with MCNP code, based on approximate 3D multigroup discrete ordinates adjoint transport solutions [9][10] generated by Denovo. The VR parameters generated by ADVANTG consist of space-energy dependent weight-window bounds (WW) and biased source distributions, which are outputted in formats that can be directly used with MCNP input [11]. ADVANTG has been applied to neutron, photon, and coupled neutron-photon simulations of real-world radiation detection and shielding scenarios [12]. ADVANTG is compatible with all MCNP geometry features and can be used to accelerate cell tallies (F4, F6, F8), surface tallies (F1 and F2), point-detector tallies (F5), and Cartesian mesh tallies (FMESH). The solution methods of ADVANTG are CADIS/FW-CADIS for generating VR parameters which provide a prescription for generating space-energy dependent WW targets and a consistent biased source distribution (SB cards in SDEF and WWINP file). The CADIS method was developed for accelerating individual tallies, whereas FW-CADIS can be applied to multiple tallies and mesh tallies.

The MCNP6.1.1b [13] is a general-purpose Monte Carlo N-Particle code that can be used for neutron, photon, electron, or coupled neutron/photon/electron transport. The MCNP treats an arbitrary three-dimensional configuration of materials in geometric cells bounded by first- and second-degree surfaces and fourth-degree elliptical tori. For neutrons, all reactions given in a particular cross-section evaluation (such as ENDF/B-VI) are accounted for. Thermal neutrons are described by both the free gas and $S(\alpha,\beta)$ models. Important standard features that make MCNP very versatile and easy to use include a powerful general source, criticality source, and surface source; both geometry and output tally plotters; a rich collection of variance reduction techniques; a flexible tally structure; and an extensive collection of cross-section data. Energy ranges are taken from 10^{-5} eV to 20 MeV for neutrons with data up to 150 MeV for some nuclides, 1 keV to 1 GeV for electrons, and 1 keV to 100 GeV for photons. Pointwise cross-section data were used within MCNP: auxiliary program MAKXSF prepares cross-section libraries with Doppler broadening.

B. MCNP simulation model

The MCNP simulation model is based on data available in reference [1] and is presented next. The reported values were taken for the neutron source inside double steel encapsulation, transport box, rabbit system, and material isotopic concentrations, while several approaches were investigated for detector tallies. Since no details exist on detector casing, the most basic approach was with point detector tally (F5) at location (100, 0, 0). This, however, puts more stringent statistical requirements on MC neutron flux convergence and loses advantage of problem spherical symmetry, which can be seen in a smaller figure of merit (FOM factor) compared to surface flux tally (F2) and volume flux tally (F4), both with radius of 100 cm. The axial cross sections of model geometry (y=0 plane) are depicted in Figure 3, while close-up view of the rabbit system housing the ^{252}Cf source is depicted in Figure 4.

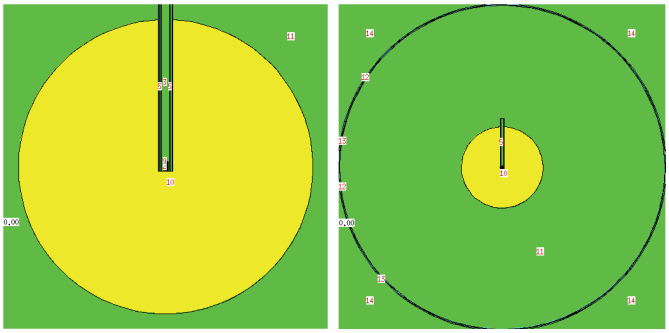

Fig. 3. Iron sphere with rabbit system and distant spherical detector (yellow-iron, green-air)

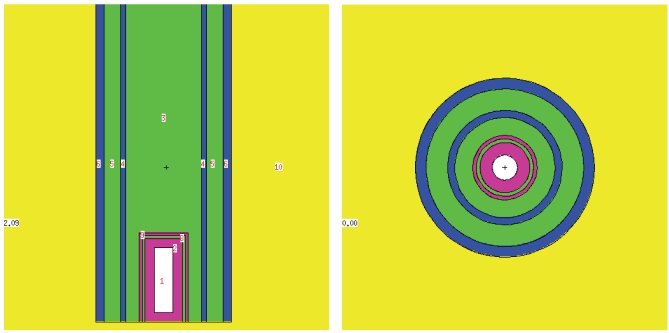

Fig. 4. Axial and radial view of the rabbit system (yellow-iron, green-air, blue-steel for tubes, purple-steel for encapsulation, white-source region)

As reported in [1], the source material is modelled as cylindrical void region (depicted in white), so to achieve a proper MC sampling, MCNP source card was defined with three independent distribution functions: radial, axial and energy. For the source energy spectrum, the MCNP built-in Watt fission spectrum of ^{252}Cf with parameters a = 1.025 MeV and b = 2.926 MeV^{-1} was replaced with a binned histogram for energy biasing, so final structure was 100 equiprobable energy bins below 6 MeV and 28 uniform bins above 6 MeV.

The neutron transport mode was the only one allowed with »mode n« option so no secondary particles (gammas) were banked. Total number of neutron histories per simulation was 100 million. The tallies in MCNP are always normalized to the source intensity of 1 n/s, while true source intensity of 125664 n/s was used for proper flux scaling and comparison with referenced values. The »FM« tally card was used to define multiplier set with a selection of:

1. proper units, i.e. barns to 1e-24 cm^2,
2. dosimetry cross sections to be used as response functions,
3. MT numbers for selecting reaction type.

This basically allows calculation of product between neutron flux and response function in integral fashion over the tally energy structure. Some point detectors without »FM« card were used only for monitoring the fast neutron flux over different energy regions, by using an »En« card, which also allowed comparison with referenced data. One specific point detector had an extra fine energy group structure (about 320 groups) to capture the neutron flux spectrum with a fine resolution. As already stated, this approach with point detectors was verified with surface flux tallies and volume flux tallies. Finally, mesh tally object (»FMESH« card) was also defined to give user a sense of global MC convergence and distribution of relative errors throughout the iron sphere to detector locations. The MC mesh had 110x110x110 cells with cell side of 2 cm.

Mario Matijević, Krešimir Trontl, Dubravko Pevec, Characterization of Fast Neutron Transmission Through an Iron Shield, Journal of Energy, vol. 72 Number 2 (2023), 8–14
https://doi.org/: 10.37798/2023722471

C. ADVANTG SIMULATION MODEL

The ADVANTG3.0.3 computer program is based on SN adjoint transport solver Denovo, so only a minimal set of typical SN input blocks is needed for input file. Using approximate SN flux solution, the VR parameters are developed that work in tandem and consist of space-energy dependent weight windows and biased source distributions. The ADVANTG3.0.3 automatically modifies »SB« cards in the »SDEF« definition part of the MCNP input and provides an external WWINP file which is read during the MC simulation.

For iron shielding problem the CADIS method was selected to optimize the neutron flux in a single localized tally located 75 cm away from an iron sphere surface. For that purpose, a point detector with different response functions was used and verified with alternate surface flux tally and surface shell volume tally. The ANISN-based multigroup library »bplus« was used with 47n/20g energy structure. The SN mesh was 110x110x110 with 2 cm cell side and ray tracing algorithm mapped materials onto mesh cells with a standard macromaterial option. Spatial discretization was step characteristic with S4/P1 parameters and diagonal transport correction for scattering cross section. Number of Krylov vectors for subspace GMRES solver was 20, maximum number of multigroup iteration was set to 100 while tolerance value was lowered to 10^{-6}. After successful run, besides generated VR parameters, ADVANTG provides very useful *.silo files to inspect quality of the SN solution with VisIt code [14]. For example, Figure 5 shows the adjoint flux solution (left) and corresponding neutron weights (right) for the first group in 47n/20g library. One can clearly notice inverse relationship between adjoint flux and particle weight, which is prescribed by CADIS method.

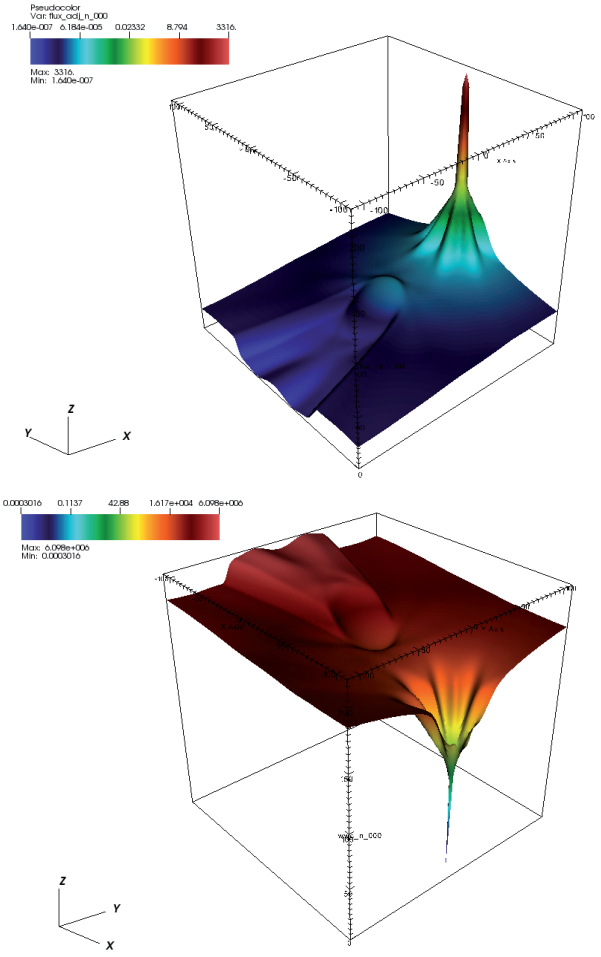

Fig. 5. Adjoint flux and neutron weights in the first group of the »bplus« library

D. IAEA REACTOR DOSIMETRY FILES

The new International Reactor Dosimetry and Fusion File (IRDFF-II) [4] addresses neutron dosimetry needs for fission and fusion applications for incident neutron energies from 0 to 60 MeV. The library includes 119 metrology reactions with covariance information and corresponding decay data. The library also includes 4 cover cross sections of B, ^{10}B, Cd and Gd used to support self-shielding corrections, 5 metrology metrics used by the dosimetry community, and 7 cumulative fission products yields. Several reference neutron fields for library validation are also provided. Finnally, recommended radionuclide masses and elemental abundances to be used for dosimetry applications are also included. The dosimetry library can be used in a broad range of applications from lifetime management and assessments of nuclear power reactors to other neutron metrology applications such as boron neutron capture therapy, therapeutic use of medical isotopes, nuclear physics measurements, and reactor safety applications. Library evaluations are based mainly on comprehensive experimental data, therefore the reaction library also represents an ideal benchmark collection for validation and improvement of theoretical nuclear reaction modelling. The older library release IRDFF-v1.05 [5] is now superseded by the new IRDFF-II library but is still used on many instances in reactor dosimetry community. Figure 6 shows high-energy reaction ^{54}Fe(n,p) from three different cross section libraries, which were used in this paper. Figure 7 shows differences in reaction ^{238}U(n,f) between IRDFF evaluations, which are quite noticeable in the resonance region. Retrieval, formatting and data plotting was done using IAEA Nuclear Data Services available at: https://www-nds.iaea.org/ [15]. The special dosimetry libraries were

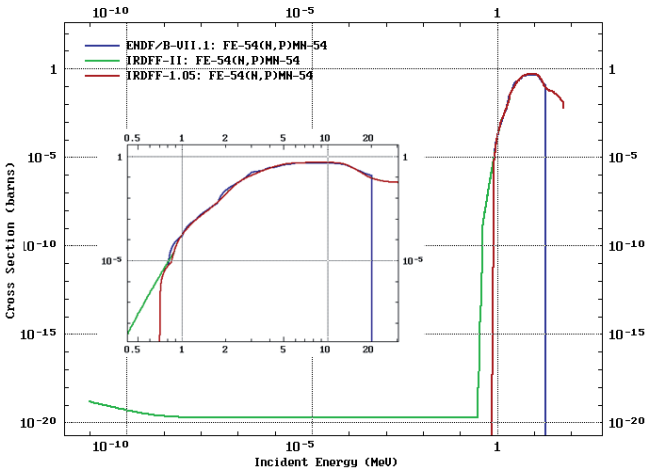

Fig. 6. Comparison of reaction 54Fe(n,p) from three different libraries

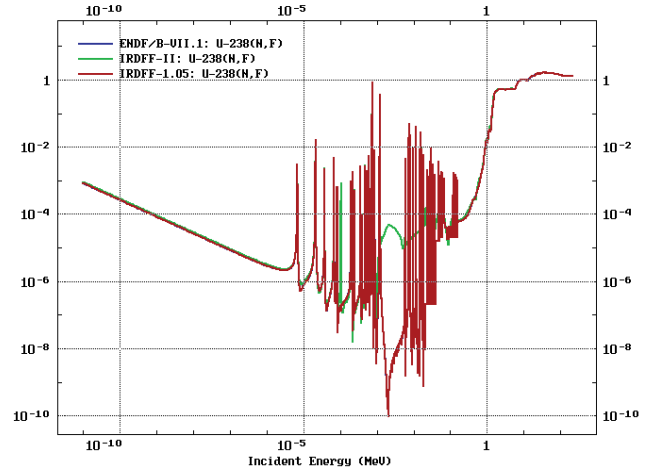

Fig. 7: Comparison of reaction 238U(n,f) from three different libraries (red covers blue)

Mario Matijević, Krešimir Trontl, Dubravko Pevec, Characterization of Fast Neutron Transmission Through an Iron Shield, Journal of Energy, vol. 72 Number 2 (2023), 8–14
https://doi.org/: 10.37798/2023722471

manually added to MCNP/DATA directory, with necessary modification of the »xsdir« files, so library selection is done through the argument »xsdir=...« in the MCNP command line.

IV. Results and Discussion

The mesh tally distribution of the fast neutron flux emerging in ambient air around the iron sphere is shown in Figure 8 together with MC relative errors. One can notice axial path of neutron streaming throughout the rabbit system which is not affecting point detector tally solution but has a marginal impact on the surface flux tally and the cell flux tally, since average neutron flux over those objects is increased. The neutron flux distribution as a function of x-axis is depicted in Figure 9, together with associated relative errors, which show steady increase up to 2% on average at detector location (r=100 cm). It is interesting to notice a change in the relative error curve profile from an exponential growth inside the iron sphere, due to strong attenuation, to a linear growth outside the sphere. The total point detector flux was found to be $7.85631 \cdot 10^{-6} \pm 0.44\%$, and after multiplying it with source intensity (125664 n/s) one obtains proper normalized value of 0.987. The total surface flux over a sphere tally with r=100 was found to be $7.8913 \cdot 10^{-6} \pm 0.00\%$. These results clearly show uniform MC convergence so additional results follow.

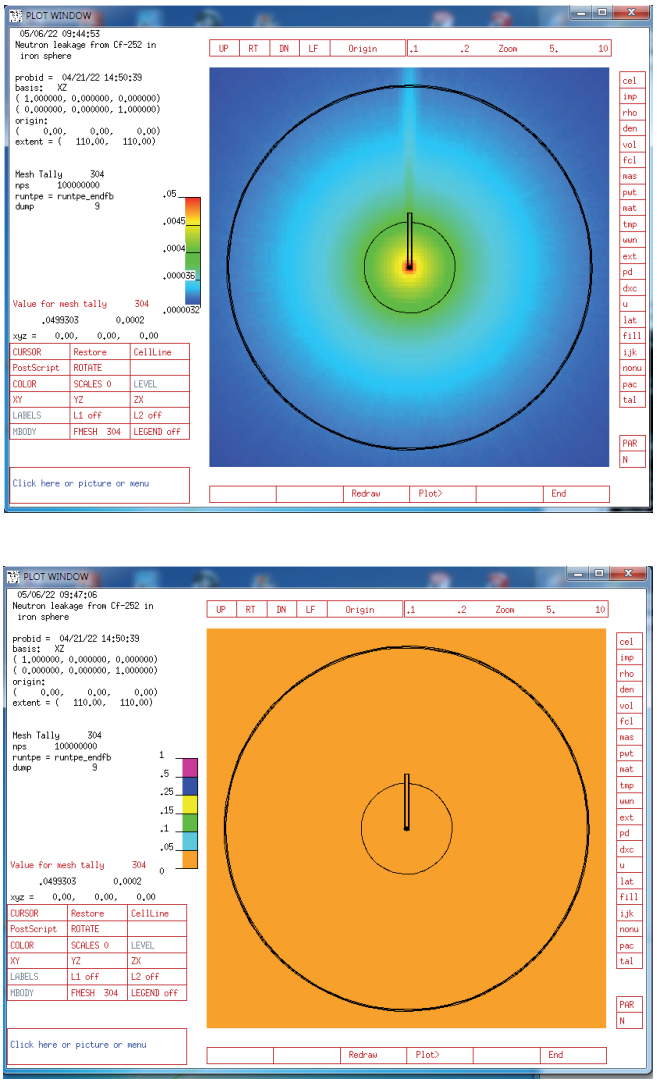

Fig. 8. Mesh tally of neutron flux in y=0 plane with relative errors

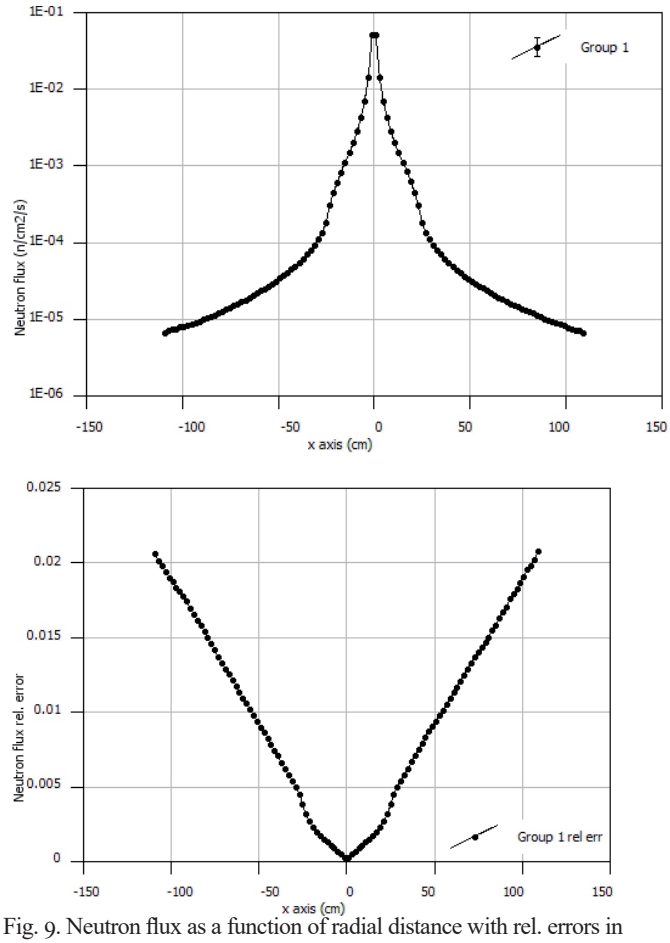

Fig. 9. Neutron flux as a function of radial distance with rel. errors in x-axis

The calculated MCNP full neutron leakage spectrum is plotted in Figure 10 in comparison with the referenced one [1], while high-energy part above 1 keV is shown in Figure 11. Below 1 keV one can notice a $1/E$ slowing down tail. A generally good agreement is obtained between MCNP and referenced results over entire spectrum domain, considering that local difference in curve variations are due to different tally energy group structure representation. However, above 1 MeV region, the spectrum solution based on ENDF/B-VII.1 evaluation shows overall higher values compared to an older ENDF/B-VI evaluation. This means that improvement in ENDF/B-VI iron data evaluation, which was first reported in [1], is also present in the ENDF/B-VII.1 iron data in predicting neutron transmission above 1 MeV. A rough assessment can be made that the same fast flux ratio of ENDF/B-VI to ENDF/B-V is also present in ratio ENDF/B-VII.1 to ENDF/B-VI evaluation. Since high-energy tail of the neutron spectrum is affecting at most high-energy dosimetry reactions, it is expected that largest difference in dosimeter reaction rates will be for reactions ^{63}Cu(n,α), ^{54}Fe(n,p) and ^{58}Ni(n,p) (see Table 1 for reaction thresholds).

The comparison of point detector fast neutron flux based on ENDF/B-VII.1 iron evaluation and its relative ratio to previous ENDF/B-VI evaluation is shown in Table 2 for different energy intervals. The total flux on point detector was $7.85631 \cdot 10^{-6} \pm 0.02\%$, and its mean value was used to calculate relative flux intensities over energy intervals. One can notice similar values for the ratios, so it is evident that fast neutron transmission in iron is even more augmented in the ENDF/VII.1 evaluation (in absolute sense). Even thought differences do exist between reaction cross sections taken from different dosimetry libraries, one must bear in mind that calculated dosimeter reaction rates represent integral energy quantities, so final results should be similar. Tables 3, 4 and 5 present detector reaction rates based on response functions taken from different libraries (ENDF/B-VII.1, IRDFF-1.05 and IRDFF-II) and

Mario Matijević, Krešimir Trontl, Dubravko Pevec, Characterization of Fast Neutron Transmission Through an Iron Shield, Journal of Energy, vol. 72 Number 2 (2023), 8–14
https://doi.org/: 10.37798/2023722471

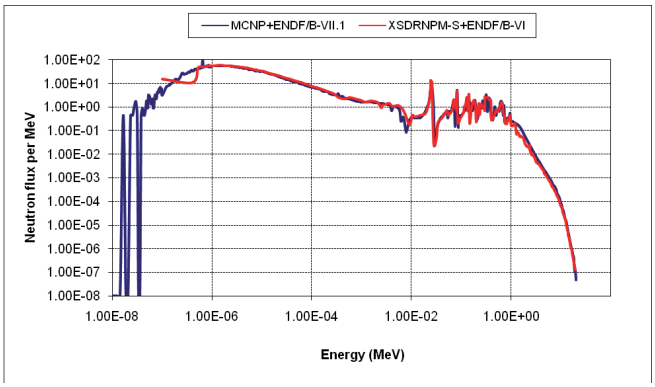

Fig. 10: Comparison of fast neutron leakage spectra in point detector

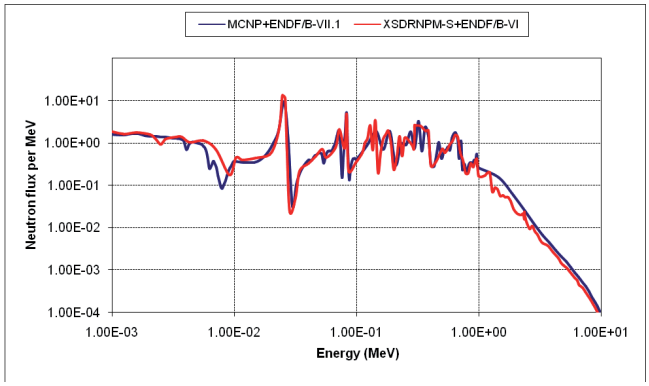

Fig. 11. High-energy detail of the neutron leakage spectra above 1 keV

comparison with original values based on VITAMIN-E dosimetry library. Overall increase in all reaction rates is a direct consequence of higher neutron transmission in ENDF/B-VII.1 transport library (above 1 MeV). The results based on IRDFF-II should be taken as relevant ones, since this library is latest and recommended by the IAEA Nuclear Data Bank.

TABLE II.

DETECTOR FAST NEUTRON FLUX OBTAINED USING ENDF/B-VII.1 TRANSPORT CROSS SECTIONS

Flux range	Response per source particle (neutron/cm²/s)	Ratio ENDF/B-VI to ENDF/B-V	Response per source particle (neutron/cm²/s)	Ratio ENDF/B-VII.1 to ENDF/B-VI
> 0.1 MeV	$8.82750 \cdot 10^{-1}$	0.996	$(7.09264 \cdot 10^{-6} \pm 0.02\%)$ $9.02799 \cdot 10^{-1}$	1.023
> 1.0 MeV	$1.05200 \cdot 10^{-1}$	1.095	$(9.86505 \cdot 10^{-7} \pm 0.05\%)$ $1.25568 \cdot 10^{-1}$	1.194
> 2.0 MeV	$2.09600 \cdot 10^{-2}$	1.173	$(2.02110 \cdot 10^{-7} \pm 0.14\%)$ $2.57258 \cdot 10^{-2}$	1.227
> 3 MeV	$7.28900 \cdot 10^{-3}$	1.289	$(7.33235 \cdot 10^{-8} \pm 0.27\%)$ $9.33307 \cdot 10^{-3}$	1.280
> 4 MeV	$3.45200 \cdot 10^{-3}$	1.341	$(3.66788 \cdot 10^{-8} \pm 0.44\%)$ $4.66871 \cdot 10^{-3}$	1.353

TABLE III

DETECTOR REACTION RATES OBTAINED USING ENDF/B-VII.1 TRANSPORT CROSS SECTIONS (RESPONSE FUNCTIONS TAKEN FROM GENERAL ENDF/B-VII.1 LIBRARY)

Reaction	Response per source particle (reaction/atom/s)	Ratio ENDF/B-VI to ENDF/B-V	Response per source particle (reaction/atom/s)	Ratio ENDF/B-VII.1 to VITAMIN-E
$^{63}Cu(n,\alpha)$	$1.55919 \cdot 10^{-34}$	1.216	$2.1700 \cdot 10^{-34} \pm 0.42\%$	1.392
$^{54}Fe(n,p)$	$2.15592 \cdot 10^{-32}$	1.229	$3.2354 \cdot 10^{-32} \pm 0.21\%$	1.500
$^{58}Ni(n,p)$	$3.52498 \cdot 10^{-32}$	1.184	$4.9932 \cdot 10^{-32} \pm 0.17\%$	1.417
$^{238}U(n,f)$	$1.93676 \cdot 10^{-31}$	1.106	$2.5149 \cdot 10^{-31} \pm 0.08\%$	1.299
$^{237}Np(n,f)$	$3.89389 \cdot 10^{-30}$	1.039	$4.4012 \cdot 10^{-30} \pm 0.03\%$	1.130
$^{59}Co(n,g)$	$3.88028 \cdot 10^{-31}$	1.267	$4.5507 \cdot 10^{-31} \pm 1.25\%$	1.173

TABLE IV

DETECTOR REACTION RATES OBTAINED USING ENDF/B-VII.1 TRANSPORT CROSS SECTIONS (RESPONSE FUNCTIONS TAKEN FROM SPECIAL IRDFF-1.05 LIBRARY)

Reaction	Response per source particle (reaction/atom/s)	Ratio ENDF/B-VI to ENDF/B-V	Response per source particle (reaction/atom/s)	Ratio IRDFF-1.05 to VITAMIN-E
$^{63}Cu(n,\alpha)$	$1.55919 \cdot 10^{-34}$	1.216	$2.2125 \cdot 10^{-34} \pm 0.41\%$	1.419
$^{54}Fe(n,p)$	$2.15592 \cdot 10^{-32}$	1.229	$3.0955 \cdot 10^{-32} \pm 0.23\%$	1.436
$^{58}Ni(n,p)$	$3.52498 \cdot 10^{-32}$	1.184	$4.7655 \cdot 10^{-32} \pm 0.18\%$	1.352
$^{238}U(n,f)$	$1.93676 \cdot 10^{-31}$	1.106	$2.5135 \cdot 10^{-31} \pm 0.08\%$	1.298
$^{237}Np(n,f)$	$3.89389 \cdot 10^{-30}$	1.039	$4.4274 \cdot 10^{-30} \pm 0.03\%$	1.137
$^{59}Co(n,g)$	$3.88028 \cdot 10^{-31}$	1.267	$4.4451 \cdot 10^{-31} \pm 0.93\%$	1.146

TABLE V

DETECTOR REACTION RATES OBTAINED USING ENDF/B-VII.1 TRANSPORT CROSS SECTIONS (RESPONSE FUNCTIONS TAKEN FROM SPECIAL IRDFF-II LIBRARY)

Reaction	Response per source particle (reaction/atom*s)	Ratio ENDF/B-VI to ENDF/B-V	Response per source particle (reaction/atom/s)	Ratio IRDFF-II to VITAMIN-E
$^{63}Cu(n,\alpha)$	$1.55919 \cdot 10^{-34}$	1.216	$2.2125 \cdot 10^{-34} \pm 0.41\%$	1.419
$^{54}Fe(n,p)$	$2.15592 \cdot 10^{-32}$	1.229	$3.0953 \cdot 10^{-32} \pm 0.23\%$	1.436
$^{58}Ni(n,p)$	$3.52498 \cdot 10^{-32}$	1.184	$4.7653 \cdot 10^{-32} \pm 0.18\%$	1.352
$^{238}U(n,f)$	$1.93676 \cdot 10^{-31}$	1.106	$2.5790 \cdot 10^{-31} \pm 0.08\%$	1.332
$^{237}Np(n,f)$	$3.89389 \cdot 10^{-30}$	1.039	$4.4385 \cdot 10^{-30} \pm 0.03\%$	1.140
$^{59}Co(n,g)$	$3.88028 \cdot 10^{-31}$	1.267	$4.4450 \cdot 10^{-31} \pm 0.93\%$	1.146

V. CONCLUSION

The RPV fluence transport calculations have indicated in the past underestimation of the dosimeter activities when using cross sections based on the ENDF/B-IV or ENDF/B-V evaluations [1]. The paper from Sajo et al [1] compares results of transport calculations based on ENDF/B-V and ENDF/B-VI evaluations, in relation to experimentally measured data for iron sphere. It was shown that for neutron energies above 1 MeV, ENDF/B-VI iron cross sections yield an increased neutron penetration through steel compared to calculations based on the ENDF/B-V. Moreover, it was noticed that the high-energy responses change by the greatest amount. The conclusion was how the ENDF/B-VI cross sections, even though improved, will not entirely resolve spectrum underestimation above 1 MeV relative to experimental data, so further refinement in iron data and/or ^{252}Cf neutron spectrum is needed.

Mario Matijević, Krešimir Trontl, Dubravko Pevec, Characterization of Fast Neutron Transmission Through an Iron Shield, Journal of Energy, vol. 72 Number 2 (2023), 8–14
https://doi.org/: 10.37798/2023722471

This paper presents continuation of this work using the MCNP code based on transport cross sections from ENDF/B-VII.1 evaluation, containing updated neutron inelastic data. The obtained fast neutron flux and detector reaction rates confirmed increased neutron transmission in iron over energies above 1 MeV, compared to SN results based on the previous ENDF/B-VI evaluation. The point detector results were verified with other tally objects, while MCNP neutron leakage spectra showed a good agreement with a reference case, except for energies above 1 MeV where it is larger on the average. This at the end produced higher reaction rates on detector by 30% to 40% for high energy threshold reactions ^{63}Cu(n,α), ^{54}Fe(n,p) and ^{58}Ni(n,p). For other reactions ^{238}U(n,f), ^{237}Np(n,f) and ^{59}Co(n,g) this increment declined to values 14% to 30%. All reactions were taken from the recommended IRDFF-II dosimetry library and produce almost the same results as reactions from IRDFF-1.05.

In addition to using the standard reaction cross section data from neutron transport libraries, MCNP provides dosimetry or activation reaction data that can be used as a response function in calculating energy integral of $\sigma(E)\phi(E)$, where $\sigma(E)$ is the microscopic cross section and $\phi(E)$ is the neutron flux. The dosimetry data libraries are appropriate only when used as a source of $\sigma(E)$ for »FM« tally multipliers, so they can't be used as a material data source for neutron transport. For this study, special dosimetry libraries IRDFF-1.05 and IRDFF-II were added to MCNP/DATA directory, replacing older built-in dosimetry data. Continuation of this work with MCNP will test the latest iron ENDF/B-VIII.0 evaluation for fast neutron transmission.

References

[1] E. Sajo, M.L. Williams, M. Asgari, »Comparison of measured and calculated neutron transmission through steel for a ^{252}Cf cource,« Annals of Nuclear Energy, Vol. 20, No. 9, pp. 585-604, 1993.

[2] M.L. Williams et al, »Transport calculations of neutron transmission through steel using ENDF/B-V, revised ENDF/B-V and ENDF/B-VI iron evaluations,« Annals of Nuclear Energy, Vol. 18, No. 10, pp. 549-565, 1991.

[3] M.B. Chadwick, M. Herman, P. Obložinsky, et al., »ENDF/B-VII.1: ENDF/B-VII.1: Nuclear Data for Science and Technology: Cross Sections, Covariances, Fission Product Yields and Decay Data«, Nuclear Data Sheets, Vol. 112(2011)2887.

[4] A. Trkov, P.J. Griffin, S.P. Simakov, L.R. Greenwood, K.I. Zolotarev, R. Capote, D.L. Aldama, V. Chechev, C. Destouches, A.C. Kahler, C. Konno, M. Kostal, M. Majerle, E. Malambu, M. Ohta, V.G. Pronyaev, V. Radulovic, S. Sato, M. Schulc, E. Simeckova, I. Vavtar, J. Wagemans, M. White, and H. Yashima, IRDFF-II: A New Neutron Metrology Library. Special issue of Nuclear Data Sheets, Vol. 163, pp. 1-108 (2020).

[5] R. Capote, K.I. Zolotarev, V.G. Pronyaev, and A. Trkov, International Reactor Dosimetry and Fusion File IRDFF v.1.05, 09 October 2014, J. ASTM International, Volume 9, Issue 4, April 2012, JAI104119

[6] T. M. Evans, A. S. Stafford, R. N. Slaybaugh, K. T. Clarno, »Denovo: A New Three-Dimensional Parallel Discrete Ordinates Code in SCALE«, Nuclear Technology, 171, 2010, pp. 171-200.

[7] J.C.Wagner and A. Haghighat, »Automated variance reduction of Monte Carlo shielding calculations using the discrete ordinates adjoint function,« Nuclear Science and Engineering, Vol. 128, no. 2, pp. 186–208, 1998.

[8] S.W. Mosher, S.R. Johnson, A.M. Bevil et al., »ADVANTG – An Automated Variance Reduction Parameter Generator,« ORNL/TM-2013/416, Rev. 1, August 2015.

[9] G. I. Bell, S. Glasstone, »Nuclear Reactor Theory«, Van Nostrand Reinhold Company, New York, 1970.

[10] E. E. Lewis, W. F. Jr. Miller, »Computational Methods of Neutron Transport«, American Nuclear Society, Illinois, 1993.

[11] M. Matijević, D. Pevec, K. Trontl, B. Petrović, "PCA Benchmark Analysis with ADVANTG3.0.1. and MCNP6.1.1b Codes", Journal of Energy: Energija, Vol. 68, No. 2-3, 2019, pp. 171-183.

[12] M. Matijević, R. Ječmenica, D. Grgić, »Spent Fuel Pool Dose Rate Calculations Using Point Kernel and Hybrid Deterministic-Stochastic Shielding Methods«, Journal of Energy: Energija, Vol. 65, No. 1, 2016, pp. 151-161.

[13] T. Goorley, »MCNP6.1.1-Beta Release Notes,« LA-UR-14-24680, 2014.

[14] »VisIt: An End-User Tool for Visualizing and Analyzing Very Large Data«, Lawrence Livermore National Laboratory, VisIt Getting Started Manual, February 2003, UCRL-MA-148506-REV-1, Version 2.7.3.

[15] IAEA Nuclear Data Services. Website: https://www-nds.iaea.org/.

Journal of Energy

VOLUME 72 Number 2 | 2023

journal homepage: http://journalofenergy.com/

A Comparative Analysis of Electric Mobility Operations in the Island States: A Case Study of Malta and Cyprus

Andy Bugeja, Brian Azzopardi, Eleftherios G. Loizou

***Summary* — The Malta and Cyprus partnership strengthened through the H2020 NEEMO (Networking for Excellence in Electric Mobility Operations) TWINNING project activities, which also led to the development of longer-term collaboration strategies for the future of electric mobility operations. Through information sharing between the two island nationsin the Mediterranean, the major goal was to improve sustainable transportation. The capacity-building activities helped to characterise the state of the two islands' electric transportation industries. Workshops, seminars, educational initiatives,andexchangevisitsareallpartofthemethodsused to increase capacity and promote collaboration. The research highlights the significance of sustainable energy sources and infrastructuredevelopmentforthesmoothtransitiontoelectric mobility and transportation. Energy systems, land transportation, and the optimisation of the entire energysystem are alldiscussed, compared and analysed. The findings highlight the legal framework, the EIRIE platform, and the differences between Malta and Cyprus in the e-mobilitysector. The integration of renewable energy in both nationsand the charging infrastructure, tariffs, and rates are also examined.**

***Keywords* — transport, electric, mobility, charging, vehicles**

I. Introduction

The transition to electric mobility is vital for addressing climate change and establishing a sustainable transportation system. This study focuses on Malta and Cyprus, two island nations with much of the same potential and obstacles in electric transportation. The project seeks to improve sustainable transportation and offer useful insights on electric mobility in island nations through information sharing and collaborative actions.The methodology used merges a project- based approach with a range of activities. Interactions and information sharing between stakeholders from Malta and Cyprus are facilitated via workshops, seminars, educational programmes, and exchange visits, which results in developing a longer-term strategy.

(Corresponding author: Andy Bugeja)

Andy Bugeja is with the MCAST Energy Research Group, Institute of Engineering and Transport, Malta College of Arts, Science and Technology (MCAST), Paola, Malta

(e-mail: andy.bugeja@mcast.edu.mt)

Brian Azzopardi is with the MCAST Energy Research Group, Institute of Engineering and Transport, Malta College of Arts, Science and Technology (MCAST), Paola, Malta and The Foundation for Innovation and Research – Malta, Birkirkara, Malta (e-mail: Brian.Azzopardi@fir.mt)

Eleftherios G. Loizou is with the Nicosia Development Agency (ANEL), Nicosia, Cyprus

(E-mail: eloizou@anel.com.cy)

The paper includes the information that was exchanged amongst NEEMO project participants. It provides an overview of the legislative framework, NEEMO's integration into the EIRIE platform, and an examination of differences between Malta and Cyprus in the e-mobility sector. Incentives for private charging service providers, the integration of renewable energy, and energy storage facilities are covered in the study. The results indicate the necessity of a robust infrastructure and environmentally friendly energy sources to meet the rising demand for electric vehicles. Additionally, the study provides insights into the policy framework, the EIRIE platform, and the potential integration of other Malta College of Arts, Science and Technology (MCAST) Energy initiatives in the future.

The NEEMO TWINNING project aims to enhance the scientific, engineering, and research capabilities of MCAST Energy Research Group (MCASTEnergy) within the MCAST Institute of Engineering and Transport (MCAST IET). By collaborating with internationally recognised research institutes, this study, which focuses on electric mobility research, helps to strengthen MCAST Energy's performance and capabilities. Through this twinning project, MCAST Energy seeks to increase its expertise and advance the studyof electric mobility.

This project involves several interactions with top scientific institutions, such as the Austrian Institute of Technology (AIT), Cyprus Energy Agency (CEA), and Nicosia Development Agency (ANEL). These alliances make it easier to connect with people in relevant sectors and gain access to a wide range of networks. Meetings, conferences, schools, seminars, and exchange programmes are among the events.To create long-term collaboration plans for electric transportation on the islands, members from MCAST and ANEL actively maintains connections between Malta and Cyprus in the electric mobility sector.

II. Methodology

The methodology combines a project-based approach with various gatherings and activities to build knowledge in e- mobility for island states. These initiatives, which seek to provide participants with a thorough understanding of the electric mobility sector in Malta and Cyprus, include workshops, seminars, education programmes, and exchange trips. The interactions between the two countries were primarily focused on identifying common requirements, difficulties, possibilities and limits in the electrictransportation sector. These interactions allowed for constructive involvement with important Cyprus and Malta stakeholders, fostering cooperation and the creation of longer- term strategies in this field. By employing this technique, the project hopes to enhance sustainable transportation by offering valuable info on how electric mobility works in island states.

Andy Bugeja, Brian Azzopardi, Eleftherios G. Loizou, A Comparative Analysis of Electric Mobility Operations in the Island States: A Case Study of Malta and Cyprus, Journal of Energy, vol. 72 Number 2 (2023), 15–19
https://doi.org/: 10.37798/2023722456

III. Result

The findings from the bilateral exchange of information between representatives from the EU-funded projectNEEMO [1] are presented in this chapter. The regulatory framework,the EIRIE platform, the integration of NEEMO inside the EIRIE platform, and an analysis of the differences between Malta and Cyprus in the e-mobility industry are outlined inthis section.

Shared data from FOSS [2] on the overall framework for encouraging electric cars and supplied data on local and thematic transport electrification, including forecasts for the deployment of electric vehicles by 2030, are shown in Fig 1 (the blue colour (bottom) represent the registration of electric vehicles, while the green colour (top) indicate the registration of electric motorbikes and motorcycles). This study also discusses incentives for private charging service providers, renewable energy versus charging stations, and electrical energy storage facilities.

A thorough knowledge of the policy framework, the European Interconnection for Research Innovation & Entrepreneurship (EIRIE) platform, and the possibility for future integration of MCAST Energy projects will be provided by discussing the specific findings generated from these exchanges and dialogues.

The PAN European Technology Energy Research Approach (PANTERA)projectalsoincludesintegratingMCASTEnergy initiatives, such as the NEEMO project, onto the EIRE platform in the future.

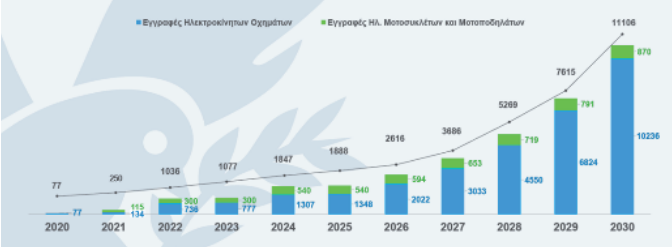

Fig. 1. Snippet from FOSS presentation - Projections of new electrical-based means of transportation. (*Blue:EVs,Green:e-Bikes*).

Furthermore, through the exchanges, MCAST and ANELwere able to exchange discussions on the following:

1. Design policies and modelling energy systems for the energy transition,
2. Current status of land transport.
3. Optimisation of the whole energy system.

Cyprus and Malta's respective renewable energy generating capacities were compared. The conversations on how the design regulations were changed in conjunction with the start of the COVID-19 epidemic and how pollution and carbon dioxide emissions were addressed. Also discussed were the similarities and differences between Malta's and Cyprus' power generation. The primary emphasis is on the following:

1. The high seasonal fluctuation in demand for power. Mainly due to summer tourists,
2. The construction of the Euro-Asia interconnector will end the isolation of the electrical grid in Cyprus.
3. Both islands have abundant solar energy, which necessitates the development of an effective system for deploying electrical storage for renewable energy sources. The construction of 50 MW of solar thermal power with eight hours of storage was proposed for Cyprus.

During the exchange programme, Cyprus Institute [3] offered Cypriot data, while some Maltese data was quoted from the National Statistics Office Malta [4]. Discussions about transportation, electric mobility, and the state of transportation in both Islands were also analysed, and Table I contains a summary of the comparison.

Table I

Fleet Comparison for Malta(MT) and Cyprus(CY) (data collected in 2021)

Fleet	Petrol		Diesel		Hybrid		Electric	
	MT	CY	MT	CY	MT	CY	MT	CY
Passenger cars	206318	541792	97067	135463	4297	9290	1488	114
Motorcycles (including scooters)	32762	57973					2126	218
Buses (route/coach/ private/ minibus)	-	-	2232	6358			11	-
Trucks	1343	6633	53555	138493	-	-	67 *	-

*Special Purpose Vehicles

Discussions and analyses of semi-fast charging station rollout planning, similar methodologies, and charging infrastructure were conducted, particularly through bilateral talks with the Cyprus Electricity Authority [5]. On similar lines, the transmission and distribution networks of Malta and Cyprus were studied. Cyprus has a 1478 MW overall generating capacity and operates independently. On the other hand, Malta has a conventional generation capacity of 380 MW and an extra 200 MW capacity that can be imported from Sicily (Italy) via an AC interconnector. Given the physical restrictions on both Islands, it is interesting that it has 132kV outgoing feeders for such a small island as Malta.

According to Reuters, in Brussels on February 14th 2023, the European Parliament enacted legislation formally outlawing the sale of new gasoline and diesel vehicles in the European Union beginning in 2035 [6]. This regulation attempts to tackle the urgent-problem of climate change while accelerating the switch to electric cars. The goal of the European Union is to promote the widespread use of electric cars and dramatically lower carbon emissions in the transportation industry, making a significant advancement towards establishing a more environmentally friendly and sustainable mobility system within the EU.

According to the ruling by the EU, CO2 emissions from automobiles and vans must beeliminated by2035. In addition, it is hoped tha tby 2030,CO2 emissions from automobiles and vans will have to be decreased by 50% from their levels in 2021. These strict regulations are designed to push the car sector toward greater sustainability and mitigate the negative effects of climate change. The legislation's aggressive emission reduction goals spur the creation and use of low- carbon technology like electric cars and alternative fuels, enabling the development of a cleaner, more environmentally friendly transportation industry.

Malta has 309,170 automobiles, assuming an annual mileage of 5,000 km per car, with 50% of the cars being converted to electric vehicles. Based on a conservative consumption rate of 0.2 kWh/km, Malta would need an additional 150 GWh of energy from the electrical system to charge the EVs. With an average annual EV trip of 7,000 km, Cyprus would require an additional 480 GWh of electricity each year.

These estimates emphasise the need for a strong infrastructure

Andy Bugeja, Brian Azzopardi, Eleftherios G. Loizou, A Comparative Analysis of Electric Mobility Operations in the Island States: A Case Study of Malta and Cyprus, Journal of Energy, vol. 72 Number 2 (2023), 15–19
https://doi.org/: 10.37798/2023722456

and sustainable energy sources to enable the transition to electric mobility by highlighting the rising need for electricity to power electric cars as they become more common in the respective countries.

The PV-based regulatory procedures and installation restrictions for Malta and Cyprus were discussed. Most photovoltaic (PV) installations are linked to the distribution network, while there are legal distinctions between PV installations on the two islands' distribution networks.

The service providers currently offer charge services have also been the subject of several discussions. The tarifffor Cyprus's e-charge service (in € per kWh) is provided in Table II. Malta's corresponding public charge rates are stated in TableIII.

Table II

Tariff (€/kWh charges) for thee-charge Service in Cyprus (CY) [7]

Year	Regular Charging (€/kWh)	Fast Charging (€/kWh)
2020	0.19	0.22
2021	0.22	0.25
January-August 2022	0.25	0.28
September-October 2022	0.37	0.40
November 2022-	0.35	0.38

ChargeMyRide [8] is the smartphone application for Malta's public EV charging. Customers of the so-called E-Drive plug charger enjoy advantageous pricing; ChargeMyRide-tariffs Malta's are listed in Table III.

Table III

Public EV Charging rates by Charge My Ride-Malta[8]

E-DrivePlug'n'ChargePackagesinMalta	
MediumCharging	FastCharging
Off-peak:€0.1698/unit	Off-peak:€0.1798/unit
Onpeak:€0.1885/unit	Onpeak:€0.1985/unit

Malta has on-peak and off-peak prices, unlike Cyprus, where the prices are constant throughout. The off-peak hours arefrom midnight to 6 am and noon to 4 pm every day on weekdays and Saturdays. On Sundays, the entire day is considered as off-peak for EV charging.

As of August 30th 2021, Enemalta [10] has been accepting applications from EV owners in Malta who wish to charge their vehicles privately in their garages. EV owners can benefit from a rate of €0.1298 per unit during off-peak hours, while on-peak hour use is subject to the appropriate electricity tariff bands. The use of the EV charger will be monitored by a separate meter. Enemalta website outlines the technical requirements for installation [11], and specific guidelines are given to address queries about electricity supply, single or three-phase requirements and EV meter installation.

Table IV

Domestic/Commercial EV Charging Tariffs in Malta (Part 1) [9]

EV Charging off-peak consumption tariff:	
Residential/Non- residential	Fixed rate of €0.1298/unit
EV Charging during peak hours tariff:	
Residential	Tariff Band Apply
Non-Residential	Fixed rateof€0.1485/unit
EV Meter Application Chargeson Existing Accounts:	
Single Phase	€50 (onetime)
Three Phase	€ 80

Table V

Domestic/Commercial EV Charging Tariffs in Malta (Part 2) [9]

Monthly Residential EV Meter Service Charge:	
Single Phase	€ 4
Three Phase	€ 6
Monthly Non-Residential EV Meter Service Charge:	
Single Phase	€ 6
Three Phase	€ 8

Compared to Cyprus's 35 cents per unit, Malta's off-peak tariff of roughly 13 cents per unit of electricity is remarkably low. If the EV energy meter is registered as non-residential in Malta, the tariff during peak hours is 14 cents per unit, but if it is registered as residential, things become complex. For residential off-peak rates, it covers the entire household's current usage, for which the applicable electricity price bands are in effect and can reach a maximum of 61 cents per unit. Additionally, one must take into account the one-time installation fees of €50 and €80 for the single and three-phase EV energy metres, respectively, as well as a monthly service fee of €6 (for single phase supply) or €8 (for three-phase supply). The client must establish a separate electrical installation for the EV Chargers to qualify for the EV energy meter. This installation might cost up to €1000, depending on the cable lengths. Of course, the estimate does not include the EV charger.

The E-Charge Service, offered by the Unit of EAC [7], is responsible for Cyprus's electric vehicle (EV) charging infrastructure. The architecture of the charging system, the communication standards, the specifications of the charging stations, the pricing scheme, and the geographic reach are all highlighted. The E-Charge Service provides Mode 3 charging while maintaining constant two-way communication between the vehicle and the charging station. The Type-2 plugs available at the charging stations allow for the simultaneous charging of two automobiles. The cost of issuing and replacing RFID cards is included in the price structure and connection and subscription fees. The E-Charge Service intends to encourage the use of electric vehicles, lower carbon emissions, and foster environmental sustainability in Cyprus.

The semi-fast charging stations installed by EAC allow charging of electric vehicles up to 21kW regular charging and 50 kW DC fast charging. Each charging station has two Type- 2 charging plugs,which can serve two vehicles simultaneously at full load.

Electric vehicle charging stations have been installed in public places covering the whole of Cyprus.The navigation map with the specific number of charging stations taken care of by EAC [7] is found in Fig 2,including the thirty-three (33) (The blue circle denotes the quantity of charging points in the area) Semi-Fast-Charging

Andy Bugeja, Brian Azzopardi, Eleftherios G. Loizou, A Comparative Analysis of Electric Mobility Operations in the Island States: A Case Study of Malta and Cyprus, Journal of Energy, vol. 72 Number 2 (2023), 15–19
https://doi.org/: 10.37798/2023722456

Station Infrastructure (22kW AC) in Cyprus.

To safeguard the environment and reduce carbon emissionsfor a better and clearer environment for Cyprus and beyond, the major goal of the e-charge service is to promote electric vehicles in Cyprus.

Malta introduced off-peak and peak rates for the public medium and fast charging stations on the island. Similar to residential charges, off-peak times are from 00:00 to 05:59 in the morning, from 12:59 to 15:59, and all day on Sundays(i.e., between 00:00 am and 11:59 pm).

Information is given on the locations of the 22kW AC semi-fast charging stations. For medium charging, the E-Drive charges are 17 cents per unit during off-peak hours and 19 cents per unit during peak hours. Fast charging costs 18 cents per unit for medium charging and 20 cents per unit for fast charging, respectively.

The charging locations can be seen in Fig 2for Cyprus andFig 3 to Fig 6 for Malta.

With approximately ten (10) pillars in Gozo and fifty (50) pillars in Malta, the EV charging service partially funded by the EU served the EV community on the islands for over a decade. The locations of the charging pillars of an old EV charging infrastructure still in use in Malta are given in Fig 3. Unlike the newly installed EV charging system,the user needs a monthly subscription for the old system in Malta, and the rates are fixed at 21 Euro cents per kWh.

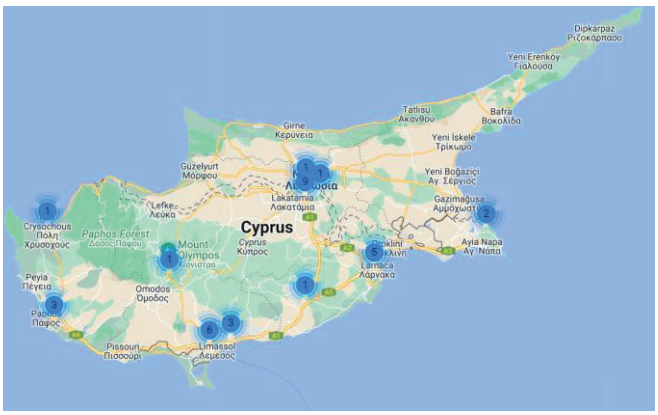

Fig. 2. The location and number of Semi-Fast-ChargingStations (22kW AC) installed in Cyprus by EAC [7].

There are three locations where one may charge an electric vehicle for free: one is in Cirkewwa next to the Gozo Ferry; another is at the port in Marsa; and a third is at the Taxbiex yacht marina. Due to the electricity from the PV panels assembled on the tent above the station, free charging is possible within the former EV charging infrastructure.

Fig. 3. Old charging station locations in Malta

All electric cars in Malta that adhere to AC (Alternating Current) charging system specifications can be charged at public charging stations. The three-phase supply used by the medium-speed AC recharging pillars can give energy up to a maximum of 22kW. For interoperability reasons, L-category electric car chargers come with two Type 2 vehicle connections, according to the standard socket outlets in EN 2- 62196.

The location of the twenty-three (23) fast chargers in Malta is given in Fig 4. The chargers also require at hree-phase supply input, thefast charging pillar installed in Malta can give DC electricity for EV charging at a maximum power output of up to 43kW.

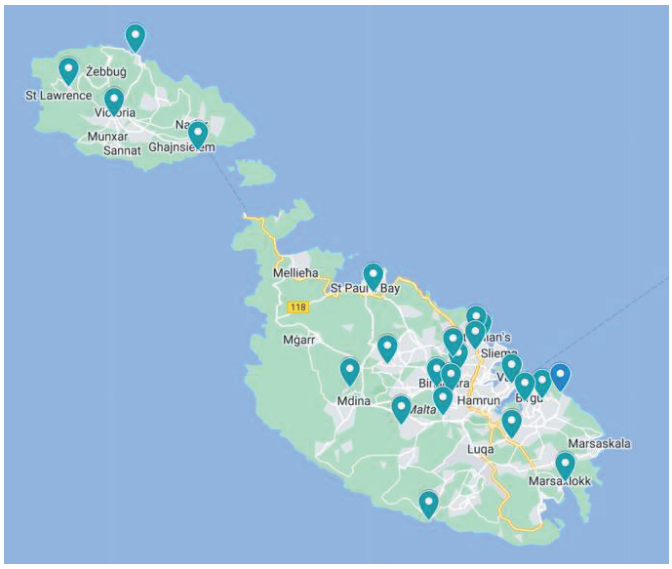

Fig. 4. Fast Charging Locations in Malta

The locations of the 30 medium DEMO chargers that are part of the recently installed EV charging infrastructure are shown in Fig 5.

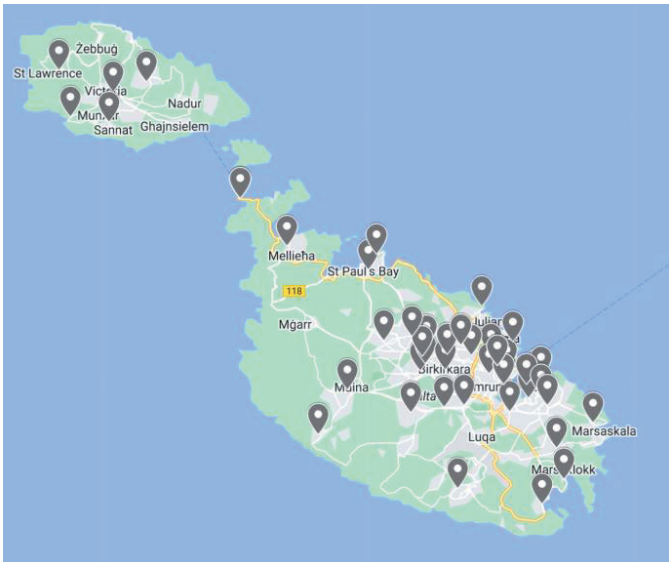

Fig. 5. Medium DEMO Charging locations in Malta

As shown in Fig 6,the newly installed EV charging infrastructure includes over three hundred eighty charging pillars in Malta.

Andy Bugeja, Brian Azzopardi, Eleftherios G. Loizou, A Comparative Analysis of Electric Mobility Operations in the Island States: A Case Study of Malta and Cyprus, Journal of Energy, vol. 72 Number 2 (2023), 15–19
https://doi.org/: 10.37798/2023722456

Fig. 6. All newly installed 384 public charging pillars in Malta

Finally, the following data on Cyprus has been compiled: reserve requirements, PV, wind, biomass, CSP, andanticipated storage technology profiles.

The losses, capacity, and operational reserves comprised most of the grid information. InCyprus, distribution losses added 3.2 per cent to the total generation, while transmission losses accounted for 1.5 per cent of the total generation. For the whole model horizon beyond 2019, a capacity reserve margin of 20% more than the annual peak demand was considered. While RET without storage was given a lesser capacity credit because of its irregular availability, storage alternatives and conventional thermal plants were permitted to contribute 100% of their rated capacity.

The operating reserves (spinning reserves), following the Republic of Cyprus's renewable energy strategy, were approved. The amount of the expressed total reserve is:

1. A constant 60 MW demand.
2. An additional 10% of PV generation and 50% of wind energy is produced instantaneously. The reserves were open to all traditional thermal methods contributions, and storage options were provided. Additionally provided was the overall annual PV generation. The annual PV profile is illustrated in Fig 7 in kWh/kWp.

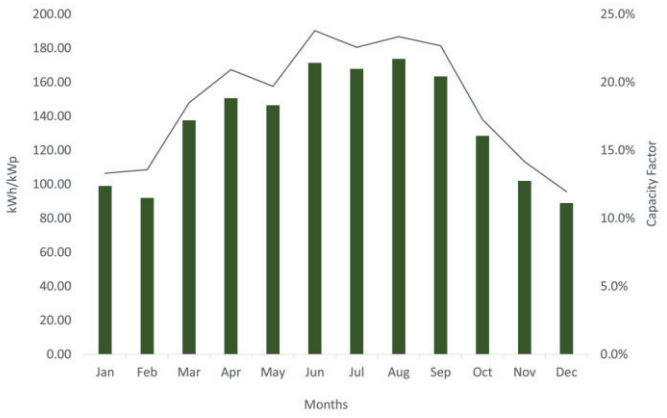

Fig.7. Plot for the PV energy produced throughout the year shared by The Cyprus Institute

IV. Conclusion

The importance of cooperation and information exchange to improve sustainable transportation is shown by the research on electric mobility conducted as part of the NEEMO project by MCAST in Malta and ANEL in Cyprus. Stakeholders from both nations engaged in constructive discussion through workshops, seminars, and exchange visits, identifying shared needs, challenges, opportunities, and limitations in the electric transportation industry.

The information exchange results between the two countries provide insight into the differencesbetween Malta and Cyprus in the e-mobility sector. The study also looks at energy generation and storage facilities and integrating renewable energy sources.

The two nations' most recent advancements in electric mobility policy, and research findings, were analysed, followed by a comparative study between the island states Malta and Cyprus.

The analysis underlines the urgent need to accelerate the transition to electric vehicles as the European Union adopts rulings to phase out gasoline and diesel automobiles by 2035. Malta and Cyprus must concentrate on infrastructure development and sustainable energy sources to fulfil the increased demand for power in light of estimates of anincrease in the adoption of electric vehicles.

Overall, this study delivers valuable info on the electric mobility market in Malta and Cyprus, aiming to improve environmentally friendly transportation. The two nations canhelp the EU in a more environmentally friendly andsustainable mobility system by exchanging information, encouraging collaboration, and implementing a longer-term strategy into action.

Acknowledgement

We would like to sincerely thank the MCAST Energy team for their invaluable assistance in familiarising themselves with the distinctive features of the study area. We want to thank ANEL from Cyprus for their remarkable contribution to this study, notably in renewable energy and electric transportation.

We also thank the Energy, Environment and Water Research Centre (EEWRC) of the Cyprus Institute, the Electricity Authority of Cyprus, the Cyprus Energy Agency, the Department of Road Transport of the Ministry of Transport Communications and Works for generously providing us with the necessary data and information. Their assistance with data and human resources has been considerable and has significantly aided in completing this study.

References

[1] "NEEMOProject–NEEMOEUH2020TWINNING Project."https://neemo-project.eu/(accessedMay29th,2023).

[2] "FOSS-UniversityofCyprus."https://fosscy.eu/ (accessed May 29th, 2023).

[3] "Home - The Cyprus Institute." https://www.cyi.ac.cy/ (accessedMay29th,2023).

[4] "NSO Malta | Access to Microdata - NSO Malta." https://nso.gov.mt/access-to-microdata/(accessedMay29th, 2023).

[5] "EAC - Κεντρική σελίδα." https://www.eac.com.cy/EN/Pages/default.aspx(accessed May 29, 2023).

[6] "EU proposes effective ban for new fossil-fuel cars from2035|Reuters."https://www.reuters.com/business/retail-consumer/eu-proposes-effective-ban-new-fossil-fuel-car-sales- 2035-2021-07-14/ (accessed May 29th, 2023).

[7] "EAC - e-charge." https://www.eac.com.cy/EN/NonRegulatedActivities/chargingstation/Pages/default1.aspx (accessed May 29th, 2023).

[8] "Charge my Ride - Plug to the future." https://chargemyride.mt/#tariffs(accessedMay29th,2023).

[9] "Electric Vehicle Charging Electricity Tariffs - Enemalta."https://www.enemalta.com.mt/electric-vehicle-charing-electricity-tariffs/ (accessed May 29th, 2023).

[10] "How to apply for an EV meter - Enemalta." https://www.enemalta.com.mt/news/apply-ev-meter/(accessed May 29th, 2023).

[11] "Application process - Enemalta." https://www.enemalta.com.mt/application-process/(accessed May 29th, 2023).

Journal of Energy
VOLUME 72 Number 2 | 2023
journal homepage: http://journalofenergy.com/

Seismic Standards Qualification of Instrument Transformers by Shake Table Test and Linear FEM Analysis

Ivan Čehil, Igor Žiger, Tomislav Capan, Matej Tuferdžić

Summary — Power grids are widely recognized as vital components of modern infrastructure. In today's society, nearly every aspect of daily life comes to a halt without electricity. Therefore, it is crucial to design power grids and their components to withstand various natural disasters. In this context, special attention is given to earthquakes and the need to enhance equipment resilience against this highly unpredictable event, which significantly impacts power grids. Instrument transformers could be the critical component in substations due to their slender design. Having this in mind, it is necessary to carry out further research and encourage development in order to reduce the impact of earthquakes on substations. Seismic qualifications are one of the means to achieve that goal. The primary objective of this paper is to share insights and experiences related to the preparation, implementation, and supervision of seismic tests conducted on a shake table. The FEM analysis, conducted as a crucial step in transformer design preparation and shake table testing, strictly adhered to the standards set by IEEE 693. IEEE 693 is widely recognized as the most demanding seismic standard regarding the substation equipment. Furthermore, the latest version of IEEE 693 was compared to other relevant standards, including IEC 61869 (current draft 38/652/CD), ETGI 1.020, and IEC 62271-300, to gain a comprehensive perspective. FEM analysis is characterized not only as a tool for design preparation and pre-test analysis but also as a valid tool for performing seismic qualifications, based on the comparison with the actual shake table tests. The paper extensively utilized the findings from seismic tests conducted on two distinct transformers, each employing different materials for critical components, in various test laboratories. These findings formed the basis for detailed analysis and conclusive insights, aligning with different versions of IEEE 693. This article aims to offer a comprehensive understanding of the seismic qualification process, providing valuable insights for substation designers, seismic specialists, and end users.

Keywords **— Seismic performance, FEM analyses, Instrument transformers, Shake-table testing, Seismic qualification**

(Corresponding author: Ivan Čehil)
Ivan Čehil, Igor Žiger and Tomislav Capan are with the Končar – Instrument Transformers, Inc., Zagreb, Croatia
(e-mails: ivan.cehil@koncar-mjt.hr, igor.ziger@koncar-mjt.hr, tomislav.capan@koncar-mjt.hr)
Matej Tuferdžić is with the Numikon Ltd., Zagreb, Croatia
(e-mail: matej.tuferdzic@numikon.hr)

I. Introduction

In the several past decades there has been a significant emphasis on overall requirements for seismic performance in the power sector. Damage due to earthquakes in seismically active regions over the last few decades was a big motivation for development of seismic standards in the US and the rest of the world [1]. The primary goal of seismic requirements for high-voltage equipment is to ensure that the entire transmission system is either unaffected or in a working state as fast as possible after a seismic event. That being said, the increased stringency of seismic standards transfers the pressure to individual component manufacturers.

In instrument transformer world, there has to be a delicate balance between the unit being designed to withstand the worst possible seismic stresses and remaining economically viable. To satisfy both ends of that spectrum, products need to be thoroughly optimized, which is a task that is difficult to perform without extensive application of FEM analysis.

This paper explains the standard seismic qualification procedure of instrument transformers and attempts to show the benefits of FEM analysis in modern product design. The usual and the widely recognized method is Response Spectrum Analysis combined with Modal Analysis [2]. Combined together, they are powerful tool for fast and efficient assessing of seismic performance.

For the purpose of this paper, two seismic qualification reports were examined, and relevant results measured during the tests were compared to the results of FEM analysis. Both analyses were done in accordance with the IEEE 693, one was made according to 2005 version of the standard and the other to 2018 version of standard. To emphasize one of the main goals of this paper, additional FEM analysis was performed with the units mounted on the support structure and with the support structure omitted (units mounted directly to the ground).

The main contribution of this paper is that it determines a solid foundation for seismic qualification of instrument transformers and practical considerations and recommendations that should be taken into account to make the entire process valid, adequate and economically feasible.

II. Comparison of Relevant Seismic Standards

It should be noted that all considered standards basically use the same terminology. Some of the more relevant terms are listed, discussed, and described in this chapter, while some of the relevant

Ivan Čehil, Igor Žiger, Tomislav Capan, Matej Tuferdžić, Seismic standards qualification of instrument transformers by shake table test and linear FEM analysis, Journal of Energy, vol. 72 Number 2 (2023), 20–26
https://doi.org/: 10.37798/2023722470

ones will be shortly discussed. *RRS (Required Response Spectrum)* is the required level of input motion for the shake table. *ZPA (Zero period acceleration)* is the largest peak value of ground acceleration and is the key parameter for determining qualification level, and for comparing different standards. *SML (Specified Mechanical Load)* is a load rating for composite insulators and one of the main criteria for acceptance of mechanical integrity in most of seismic standards. This is a maximum load which the composite insulator has to withstand for one minute [3].

There are several seismic standards available worldwide. Probably the most well-rounded and the most demanding is the IEEE 693, which is still present in the market in its 2005 and 2018 variants [4], [5]. It covers a wide range of high voltage equipment, including instrument transformers. It is applied mostly in North America and approved in numerous countries across the world.

IEC 62271-300 is primarily intended for circuit breakers and is found to be one of the less demanding standards [6]. This fact was taken into account and addressed by a new revision of IEC 61869-1 (current draft 38/652/CD), which will contain a specific annex for seismic qualification of instrument transformers, due to their specific design [7].

ETGI and ETGA are Chilean engineering standards [8]. Due to very high seismic hazards and the strongest recorded earthquakes, Chile is one of the most seismic active regions of the world. For ETGI and ETGA there is only one qualification level. As an alternative standard in Chile, there is a recommendation to use high performance level of IEEE 693 [8].

Table I provides an overview of the most commonly used seismic standards. Furthermore, Figure 1 shows the comparison of RRS for ZPA = 0,5g, which in this case corresponds to IEEE 693:2018 High design level [3], [4]. Based on this, it immediately evident that IEEE 693:2018 is the most demanding standard with the greatest accelerations which should result with the biggest loads applied on the tested equipment.

Since ETGI standard allows equivalent qualification according to IEEE 693 and IEC 62271-300 will soon be superseded by the new revision of IEC 61869-1, which will specifically cover instrument transformers, it makes sense to focus further on comparison between these two standards. The comparison of different RRS requirements is shown in Figure 2. As a first remark in the comparison of those two standards, it has to be noted that the new revision of IEC will use the same RRS as IEEE. The biggest difference between IEEE and IEC is that IEEE in its latest revision from 2018 makes it mandatory to use the three axes in testing and dynamic analysis while IEC doesn't. Furthermore, what can be seen in the Figure 2 is that the IEEE standard does have a 1,0g level and with 2018 revision, this becomes the golden standard for testing, while IEC only have up to 0,5g. The corresponding test levels specified by the IEEE 693 standard are more stringent than those proposed in IEC 61869-1. The only moot point is the 0.3g level according to IEC, which is theoretically more demanding than moderate design level, based on RRS alone. This fact is analysed in more detail and presented in Table II, which presents the proposed equivalency levels from IEEE 693:2018 which can be inherently applied to IEC required levels, but not vice versa.

IEC does not require qualification for voltage levels below 72,5 kV, so any existing qualification according to IEEE 693 should be ineherently valid. Similarly, any qualification performed for units that are of 245 kV voltage level or higher, should be done by actual seismic testing, according to IEEE 693:2018 [4]. That leaves only units that are rated between 72,5 and 170 kV which should be qualified by dynamic analysis according to IEEE, while IEC allows both static and dynamic analysis. That being said, the only range where IEEE is not obviously applicable is for units rated between 72,5 kV and 170 kV for required level of 0,3g. However, since the IEC standard has different requirements that are much more lenient than IEEE, such as aforementioned two axes instead of three, 0,5g instead of 1,0g, lower vertical acceleration factor (0,5 vs 0,8), superelevation factor (1,5 vs. 2,5), no requirement on conductor load, no additional tests for insulators required (e.g. shed seal test for composite insulators) and a lower safety margin on the insulators, it can be concluded that it is universally less stringent than IEEE 693:2018. Furthermore, today there are not many customers who want to have the equipment that can fulfill 0,3g or lower accelerations, almost everyone will demand the 0,5g whether they need it or not. This leaves manufacturers with no choice but to fulfill the most stringent requirement. On 0,5g level, there is no doubt that IEEE is more demanding and better-rounded standard than IEC. A couple of published papers thematizes the need for harmonization between different seismic standards and recognizes the IEEE in general as the most demanding standard [14], [15].

TABLE I

COMPARISON OF THE MOST USED SEISMIC STANDARDS

Standard	Qualification level [g]	Acceptance Criterium	Safety factor
IEEE 693-2018	Design Level: 1. Low: ZPA≤0,1 2. Moderate: ZPA=0,3 3. High: ZPA=0,5	Ductile materials: ≤ yield strength/ Ω (AISC 360, ASD) Brittle materials: ≤ 50% breaking strength (SML)	1,67 2,0
	Performance Level: 1. Low: ZPA≤0,1 2. Moderate: ZPA=0,5 3. High: ZPA=1,0	Ductile materials: ≤ yield strength / Ω (AISC 360, ASD) Brittle materials: ≤ 100% breaking strength (SML)	1 1
IEC 62271-300	Low: ZPA≤0,2 Moderate: ZPA=0,3 High: ZPA=0,5	Ductile and Brittle materials: ≤ 100% Yield strength	1
IEC 61869-1 38/652/CD	Very light: ZPA=0,1 Light to medium: ZPA=0,2 Medium to strong ZPA=0,3 Strong to very strong: ZPA=0,5	Ductile materials: ≤ 100% yield strength Brittle materials: ≤ 100% breaking strength	1
ETGA (ETGI) 1-0.20	0,5	Ductile materials: ≤ 80% yield strength	1,25 2
		Brittle materials: ≤ 50% breaking strength	

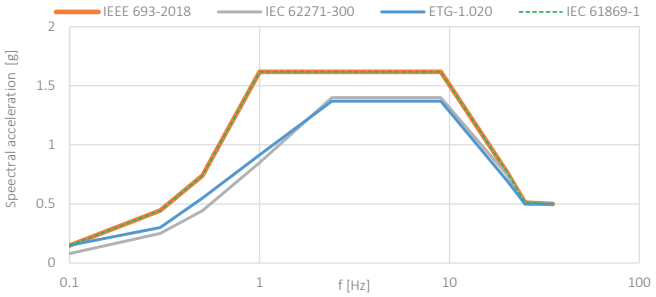

Fig 1. Comparison of RRS present in different standards for ZPA = 0,5g

Fig. 1. Comparison of RRS present in different standards for ZPA = 0,5g

Ivan Čehil, Igor Žiger, Tomislav Capan, Matej Tuferdžić, Seismic standards qualification of instrument transformers by shake table test and linear FEM analysis, Journal of Energy, vol. 72 Number 2 (2023), 20–26
https://doi.org/: 10.37798/2023722470

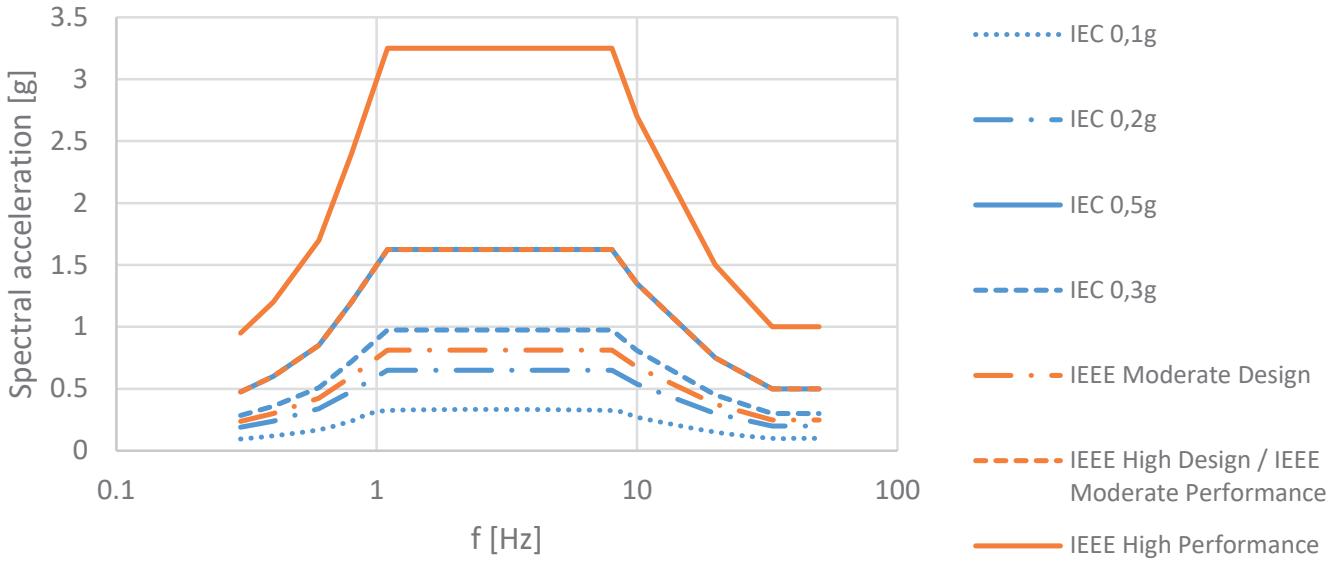

Fig. 2. Comparison of RRS between IEEE 693:108 and IEC 61869-1 (38/652/CD)

TABLE II

QUALIFICATION EQUIVALENCY BETWEEN IEEE 693:2018 AND IEC 61869-1

Voltage class [kV]	IEC Seismic level [g]			
	0,1	0,2	0,3	0,5
< 72,5	IEEE Low	IEEE Moderate	IEEE Moderate	IEEE High
72,5 – 170	IEEE Low	IEEE Moderate	IEEE Moderate	IEEE High
≥ 245	IEEE Low	IEEE Moderate	IEEE Moderate	IEEE High

Based on the comparison presented in this chapter, it can be stated that instrument transformers which satisfy the IEEE 693 standard, at the same time satisfy standards IEC 62271-300, IEC 61869-1 and ETG-1.020 (High Performance level), which is a very important conclusion, crucial for recognition and approval of existing test reports, especially because instrument transformers are the type of equipment that is not economically justifiable to be tested for the same requirement due to a cosmetic difference between available standards.

III. UNITS CONSIDERED AND TESTING PERFORMED

There has to be made some clarifications about the process of the qualification according to IEEE 693. Both 2005 and 2018 versions require shake table test during which strains has to be measured on the critical points of structural components. The test itself has some specifics, there has to be certain enveloping of the spectra which requires testing starting at a lower percentage of the RRS and going up to the 100% of required RRS. The number of these steps can vary between different testing laboratories and their best practice. The danger in doing to many steps and repetitions is that the test objects can be unnecessarily loaded, increasing the risk of damage before the main test itself. The authors strongly recommend only the necessary steps before the main test itself. Main test is performed only once and maximum strains, accelerations and deflections are measured during this main test.

All further analysis performed take two distinct transformers into account. The first one is a combined instrument transformer type VAU-245 [9]. Transformer base assembly is made from structural steel and the insulator material is porcelain. The transformer VAU-245 was tested in IZIIS, Skopje, per IEEE 693-2005 standard, mounted on a steel support structure. The unit contained a porcelain insulator. Transformer has successfully been qualified to the High Seismic Qualification Level with ZPA=0,5g of RRS according to the IEEE 693-2005. Since the laboratory is equipped with bi-axial shaking table (one horizontal and one vertical axis), and during bi-axial test, it was shown that a significant coupling exists and the transformer was tested with horizontal acceleration increased by a factor of 1.4, according to IEEE 693-2005 A.1.1.2.2. [5]

The test method consisted of resonant frequency search tests and bi-axial time history shake table testing. Bi-axial time history tests were carried out with simultaneous but independent inputs into the horizontal Y and vertical Z axes, each producing the High Required Response Spectrum (RRS). Results are shown and compared with FEM analysis in the next chapter. Figure 3 shows the applied TRS (Test Response Spectrum) against the RRS.

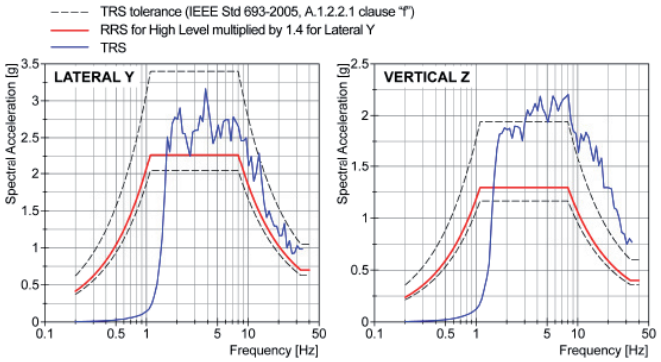

Fig. 3. Input time history (Random) and TRS vs RRS for VAU-245

Fig. 3. Input time history (Random) and TRS vs RRS for VAU-245

Figure 4 shows the seismic outline drawing made for the tested transformer with all relevant data.

Ivan Čehil, Igor Žiger, Tomislav Capan, Matej Tuferdžić, Seismic standards qualification of instrument transformers by shake table test and linear FEM analysis, Journal of Energy, vol. 72 Number 2 (2023), 20–26
https://doi.org/: 10.37798/2023722470

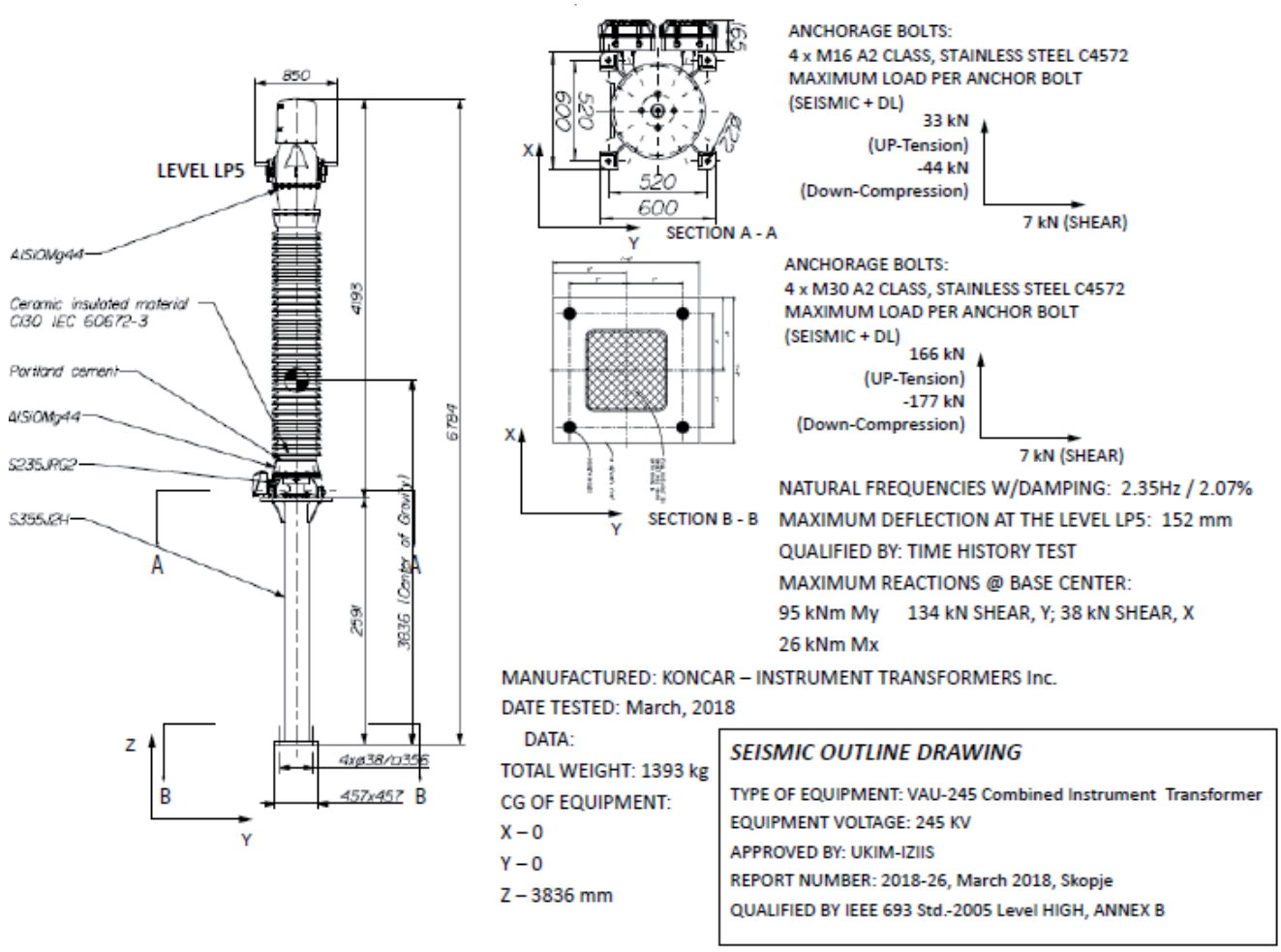

Fig. 4. Input time history (Random) and TRS vs RRS for VAU-245

The second tested transformer was an inductive voltage transformer type VPU-145 [10]. The transformer was tested in CESI laboratory, Italy per IEEE 693-2018. The unit had a composite insulator and was tested mounted on a steel support structure. Transformer has been qualified to the High Performance Seismic Qualification Level with ZPA=1g of RRS according to the IEEE 693-2018.

Laboratory is equipped with tri-axial shaking table. The test method consisted of resonant frequency search tests and tri-axial time history shake table testing. Tri-axial time history tests were carried out with simultaneous but independent inputs into the horizontal X and Y, and vertical Z axes, each producing the High Required Response Spectrum. Results are shown and compared with FEM analysis in the next chapter. Figure 5 shows the applied TRS (Test Response Spectrum) against the RRS.

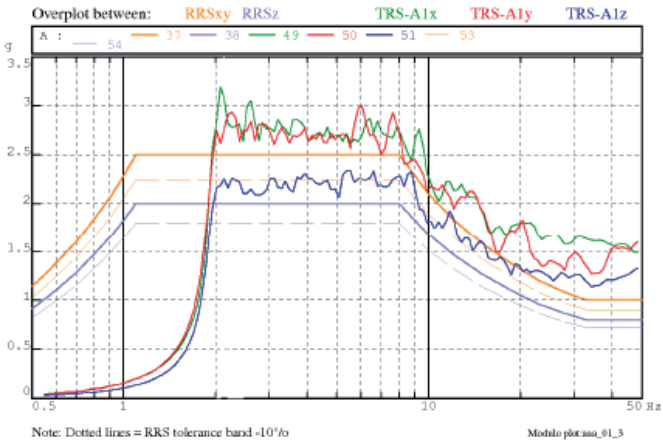

Fig. 5. Input time history (Random) and TRS vs RRS for VPU-145

Figure 6 shows the seismic outline drawing made for the tested transformer with all relevant data.

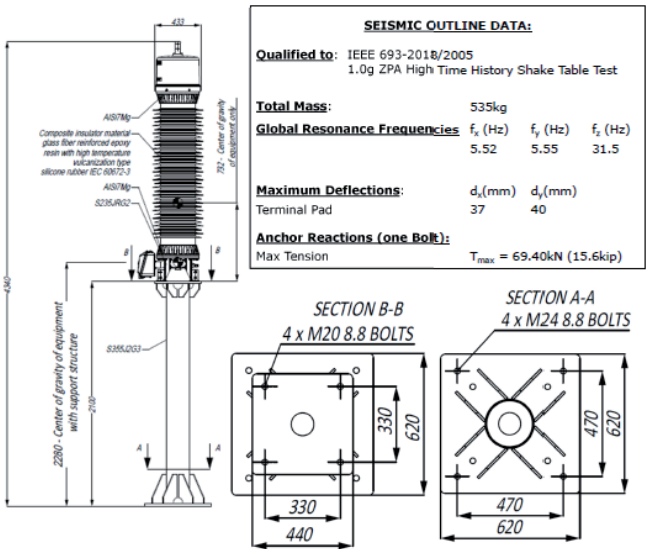

Fig. 6. Input time history (Random) and TRS vs RRS for VPU-145

Ivan Čehil, Igor Žiger, Tomislav Capan, Matej Tuferdžić, Seismic standards qualification of instrument transformers by shake table test and linear FEM analysis, Journal of Energy, vol. 72 Number 2 (2023), 20–26
https://doi.org/: 10.37798/2023722470

IV. FEM Analysis and Results Comparison

FEM analysis is advised to be used both as pre and post analysis of shake table tests. In both cases, the main goal is a better understanding of instrument transformers' dynamic behaviour. As a powerful tool, FEM analysis provides an opportunity for design iterations which can result in a well-optimized product. The main goal of this paper was to present the results from seismic shake table testing for two different instrument transformers with different insulator material and compare them with the FEM analysis performed on those two transformers. As mentioned earlier, Response Spectrum method in combination with Modal analysis was used [3].

The comparison of results from FEM analysis and shake table tests are shown in Table III. As it can be seen, there is a good relation between the test shake table results and FEM analysis, with the maximal difference within 15%. Furthermore, and adequate matching of natural frequencies in both transformers is observed, which is typically an indication of a correctly implemented model.

One of the results that attention should be paid to is the stress on the insulator, which exhibited good correlation for both considered cases. Porcelain is a brittle material and mechanical properties are determined by the manufacturer technology. Generally speaking, the more controlled and automated the production process is, the more predictable the properties of porcelain are [11]. This is extremely important since IEEE 693 and other standards define safety factors for porcelain insulators based on standard deviation of the breaking force. If the standard deviation is high, achieving certain force results with the higher insulator mass and it affects the behaviour of whole transformer.

Both materials are anisotropic, so to reduce the computing time a homogenous material must be created. For composite insulators, different moduli of elasticity for all three different axes were implemented. All data used in the analyses was supplied by the manufacturer, obtained on similar insulators, which could lead to certain discrepancies between shake table tests and FEM analyses. Still, those discrepancies are well within acceptable limits.

The comparison of actual test to the calculated data for combined unit type VAU-245 and inductive voltage transformer VPU-145 is shown in Figure 7 and Figure 8, respectively.

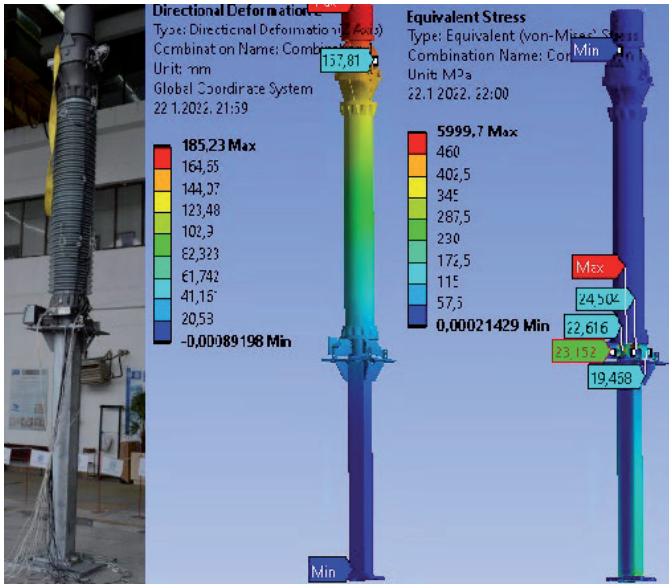

Fig. 7. VAU-245 in test and FEM analysis

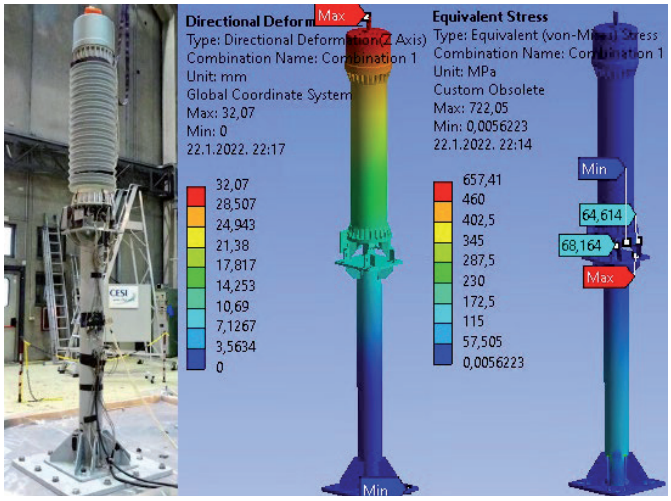

Fig. 8. VPU-145 in test and FEM analysis

One of the main points of this paper is to suggest that any unit should be qualified with an included support structure. It is clear that in some cases the actual structure it will be mounted on is not known at the time of design. Even then, a more realistic representation of the unit's behaviour will be obtained if it is considered with a default structure than no structure at all. The same recommendation is corroborated by data shown in Figure 9.

Table III

Comparison of shake-table testing and performed FEM analyses for both units

	VAU-245				VPU-145			
	Natural frequency [Hz]	Base assembly stress [MPa]	Insulator stress [MPa]	Directional deformation [mm]	Natural frequency [Hz]	Base assembly stress [MPa]	Insulator stress [MPa]	Directional deformation [mm]
Shake table test	2,35	21	14,3	152	5,55	74,4	10,93	37
Response Spectrum method	2,27	24	14,8	158	5,61	68,2	9,5	32
Difference [%]	3,5	13,3	3,4	3,9	1	8,7	14	14,5

Ivan Čehil, Igor Žiger, Tomislav Capan, Matej Tuferdžić, Seismic standards qualification of instrument transformers by shake table test and linear FEM analysis, Journal of Energy, vol. 72 Number 2 (2023), 20–26
https://doi.org/: 10.37798/2023722470

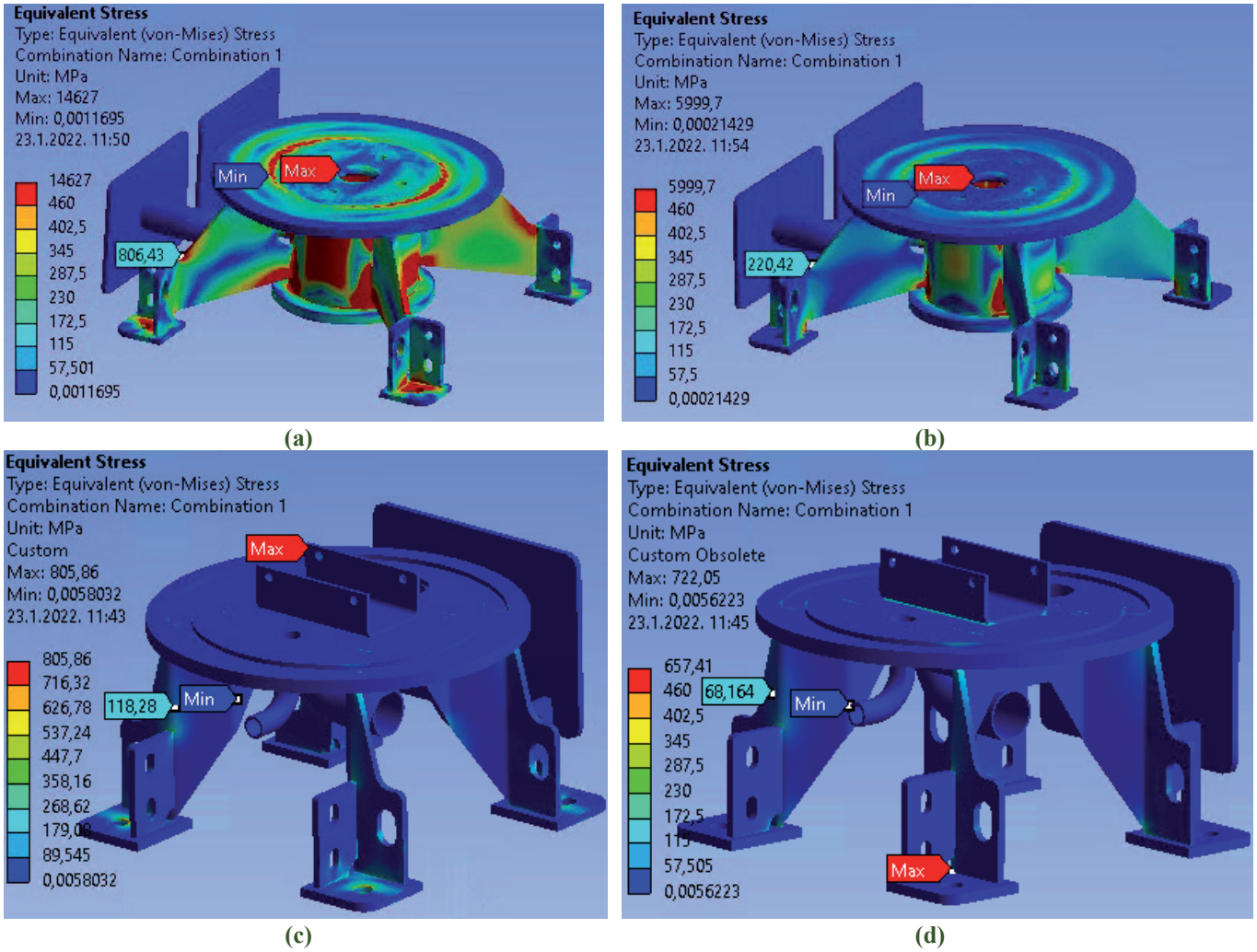

Fig. 9. Comparison of equivalent stress for CTVT Type VAU-245: (a) CTVT Type VAU-245 without steel support structure (b) CTVT Type VAU-245 with steel support structure (c) VT Type VPU-145 without steel support structure (d) VT Type VPU-145 with steel support structure

As it can be seen in Figure 9, in a critical area in VAU-245 base assembly exhibited a stress concentration which is almost two times higher than ultimate tensile stress and in terms of absolute change at this point, stress is almost four times higher than in analysis with support structure. In case of VPU-145, there is similar relation between results. This only means that the design of the unit has to be overdimensioned in a location that would not be exposed to this type of stress in actual operating conditions (i.e., with the unit mounted on a support structure).

Moreover, per clause 5.10.4 of IEEE 693-2018 standard, when tests or analyses must be carried out without support structure, the input accelerations have to be multiplied with a factor of 2,5 [4]. Table III shows the comparison of results of FEM analysis with and without support structure, obtained at the same measurement points in order to see how it affects the whole structure, not just steel base assembly. As expected, there is a huge difference between results with support structure and without.

Almost all calculated values for VAU-245 mounted directly without a support structure present are more than two times higher than those with support structure. VPU doesn't follow the same relations since it has much lower weight, center of gravity and a composite insulator. However, there are also visible increases in stress, especially in the base assembly. For those reasons, the authors strongly recommend that testing should be done with the support structure in order to avoid such situations.

TABLE IV

COMPARISON OF FEM RESULTS WITH AND WITHOUT SUPPORT STRUCTURE FOR BOTH UNITS

	VAU 245		VPU 145	
	Base assembly stress [MPa]	Insulator stress [MPa]	Base assembly stress [MPa]	Insulator stress [MPa]
FEM with support structure	220	14,8	68,2	7,15
FEM without support structure	806	33,5	118,3	7,7
Increase [%]	266	126	73	7,7

It should be mentioned that the comparison of test results and Response Spectrum method does introduce some uncertanties, primarily due to a different nature of testing and Response Spectrum method. Tests can be considered as a nonlinear transient real-life analysis while Response Spectrum method is a linear method derived from time history analysis [12]. It uses input as a maximum response of SDOF (Single Degree of Freedom) systems of time dependent loads [13].

Ivan Čehil, Igor Žiger, Tomislav Capan, Matej Tuferdžić, Seismic standards qualification of instrument transformers by shake table test and linear FEM analysis, Journal of Energy, vol. 72 Number 2 (2023), 20–26
https://doi.org/: 10.37798/2023722470

In addition, shake tables are enormously complex and massive hydraulic systems, with obvious tolerances and limitations on their performance, which can result in different TRS (Test Response Spectrum) than expected one which can over test the transformer (it is usual to have rises and drops of signal which results with non-uniform time history plot).

Consequently, it is expectable to have certain deviations between the shake table tests and Response Spectrum method. As another way to ensure the reliability of the results, there is a nonlinear Time History method which can deliver even better results than Response Spectrum [3].

V. Conclusion

There are three main conclusions to this paper, which were corroborated by comparisons of different standards, tests and FEM calculations.

The first conclusion is that the preferred standard for seismic qualification should be IEEE 693:2018 as it gives the most well-rounded, stringent requirements and recommendations as well as standardized requirements on documentation and contents of each report. The upcoming revision of the IEC 61869-1 standard (i.e., 38/652/CD) introduces a worthwhile approach where all requirements are included in a product-specific standard. However, it is lacking in many areas, compared to the IEEE 693. For that reason, any qualification performed according to IEEE 693 should be inherently applicable to the requirements of the IEC standard, which will hopefully be recognized by the international experts.

The second conclusion is that FEM analysis can be used as a reliable tool both for design qualification and design optimization. Actual testing results obtained for two units with different parameters, materials and testing standards were compared to FEM analysis and displayed a good correlation.

The final conclusion of the paper is that instrument transformers should always be qualified with support structures. If actual support structures are not known or available, the units should be qualified with default, manufacturer-recommended structures. The rationale is, even with a different support structure, the results and stress distribution are more representative to actual operating conditions than units tested directly on the ground surface with a super-relevation factor applied. In laymans terms, qualification without a support structure places an inappropriate amount of stress where it normally would not be.

This paper is aimed to serve as a fundamental guideline for adequate interpretation of different standard requirements and a basis for further research in seismic performance of instrument transformers, which is a fast-evolving topic in the expert community in recent years.

References

[1] E. Fujisaki, S. Takhirov, Q. Xie, K. M. Mosalam, "Seismic Vulnerability of Power Supply: Lessons Learned from Recent Earthquakes and Future Horizons of Research" 9th International Conference on Structural Dynamics, EURODYN 2014, Porto, Portugal, 30 June-2 July 2014.

[2] M. Fragiadakis, "Response Spectrum Analysis of Structures Subjected to Seismic Actions" Encyclopedia of Earthquake Engineering, 2013.

[3] I. Čehil, I. Žiger, T. Capan, M. Tuferdžić: "Design Safety Assesment of Instrument transformers in seismically active regions", 15th Session of HRO CIGRE, Šibenik, Croatia, 7-10 November 2021

[4] IEEE 693-2018, IEEE Recommended practice for seismic design of substations, 2018.

[5] IEEE 693-2005, IEEE Recommended practice for seismic design of substations, 2005.

[6] IEC 62271-300, High-voltage Switchgear and Controlgear – Seismic Qualification of Alternating Current Circuit-Breakers, 2006.

[7] 38/652/CD IEC 61869-1 ED2, "Instrument Transformers - Part 1: General Requirements" Committee Draft, 2021

[8] ETGI (ETGA) - 1.020, General technical specifications - Requirements for Seismic Design of Electrical Equipment, 1997.

[9] M. Poljak, B. Bojanić, V. Ravlić, "Combined Transformer type VAU, Optimal Solution for HV Substation, Power Industry, Vol. 79, pp. 27-30, 2002.

[10] I. Žiger, D. Krajtner, Z. Ubrekić, "Pushing the Boundaries of Inductive Voltage Transformer Design", 3rd International Colloquium Transformer Research and Asset Management, Split, Croatia, 15-17 October 2014.

[11] P. Maloney, "Improving Performance of Porcelain under Seismic Conditions", Insulator News and Market Report (INMR) World Congress, Munich, Germany, October, 19-21 October 2015

[12] P. Chandrakar, P. S. Bokare: "A review - Comparison between Response Spectrum Method and Time History Method for Dynamic Analysis of Multistoried Building", International Journal of Science and Research (IJSR), Vol. 6, No. 5, pp. 244-247, May 2017

[13] M. Sivy, M. Musil, "Comparison of Time-History and Spectrum Analysis of Flexible Liquid Storage Tank for Seismic Excitation using FEM approach", The 21st International Acoustic Conference: Noise and Vibration in Practice, Kočovce, Slovak republic, Vol. 21, 30-31 May 2016

[14] C. Kotanidis, A. Palaiochorinou, H. Koch, "Overview of Major Seismic Standards for High Voltage Electrical Equipment. Proposal for Harmonization of IEC 62271-207 with IEEE 693", 16th European Conference on Earthquake Engineering (16ECEE), Thessaloniki, Greece, 18-21 June 2018

[15] Z. Guan, Q. Zhu, X. Fan, M. Cao, B. Yuan, H. Wang, J. Ren, "Comparison and Research on Seismic Design Practice for Electric Substation Equipment in China, Japan, USA, and Europe", 2018 2nd International Workshop on Renewable Energy and Development (IWRED 2018), IOP Conference Series: Earth and Environmental Science, Vol. 153, No. 4, 2018

ENERGIJA